JFM PAPERS

Bragg scattering of nonlinear surface waves by sinusoidal sandbars

Haiqi Fang[1]**, Lian Tang**[1],†ᵈ **and Pengzhi Lin**[1],†

[1]State Key Laboratory of Hydraulics and Mountain River Engineering, Sichuan University, Chengdu 610065, PR China

Based on the multiple-scale expansion technique, a new set of extended nonlinear Schrödinger (ENLS) equations up to the third order is derived to account for the additional high-order bottom and dispersion effects as well as the nonlinear wave interaction on wave transformation over periodic sandbars of sinusoidal geometry. By employing the small-amplitude wave assumption, a closed-form analytical solution for Bragg scattering is obtained from the linearised ENLS equations, which demonstrates that a downshift of wave frequency of the maximum reflection is mainly due to the inclusion of the high-order bottom effect. The factors that affect the downshift of the resonant frequency are identified and a theoretical expression in parabolic form is derived to quantify the downshift magnitude. The fully ENLS equations are further analysed to reveal the additional wave nonlinear effects on Bragg scattering characteristics. Under the condition of infinitesimal sandbar amplitude, the ENLS equations render a theoretical expression of the critical value of kh when the nonlinear wave self-modulation effect and the nonlinear wave cross-modulation effect are equal, whereas the former effect is responsible for wavenumber upshifting and the latter downshifting. When kh is larger than the critical value, the increase of wave nonlinearity will enhance the downshift magnitude of the Bragg resonance, and vice versa. For finite amplitude of the bottom sandbar, the ENLS equations are solved numerically to examine the influence of both wave nonlinearity and sandbar amplitude on the characteristics of Bragg resonance. The results reveal that as the increase of sandbar amplitude, the critical kh increases monotonically.

Key words: wave scattering, surface gravity waves, coastal engineering

1. Introduction

The Bragg resonance phenomenon, characterised by the partial reflection and transmission of incident waves over sinusoidal sandbars, exhibits the maximal reflection when the wavelength of the incident wave (λ) is approximately twice the wavelength of the sandbar undulations (λ_d). Initially confirmed in the laboratory by Davies & Heathershaw

† Email addresses for correspondence: tanglian@scu.edu.cn, cvelinpz@scu.edu.cn

(1984), the phenomenon was further studied experimentally, particularly in relation to wave–current interactions, by Magne, Rey & Ardhuin (2005) and Laffitte *et al.* (2021). The higher-order Bragg resonance under more complex resonance conditions has been investigated by Guazzelli, Rey & Belzons (1992) and Peng *et al.* (2019) through experimental measurements. The Bragg resonance phenomenon has usually been utilised to design artificial bars for coastal protection (Mei, Hara & Naciri 1988; Kirby & Anton 1990; Liu, Luo & Zeng 2015).

Wave scattering theories have been widely used to explain the Bragg resonance phenomenon. The full nonlinear potential flow theory, incorporating surface and bottom nonlinearity, is capable of accurately describing wave scattering. However, numerical approaches are required to solve the equations, as shown by Liu & Yue (1998) and Peng *et al.* (2019). To explore the analytical solutions or obtain simplified models, other water wave equations with different assumptions are employed. Starting from the surface-linearised Laplace equation, the analytical solutions including Floquet solutions (Howard & Yu 2007; Yu & Howard 2012) and perturbation solution (Davies & Heathershaw 1984) are derived.

By further assuming a wavenumber varying with water depth, the surface-linearised Laplace equation can lead to the mild-slope-type equations (Berkhoff 1973; Kirby 1986*a*; Chamberlain & Porter 1995). Kirby (1986*a*) developed extended mild-slope equations by dividing the seabeds into two components that vary slowly and rapidly, which provided an effective method to deal with arbitrary geometries of one- and two-dimensional topography directly. In addition, the mild-slope-type equation has been extended to include the third-order nonlinear effect for Stokes waves where only the forward mode is considered (Kirby & Dalrymple 1983, 1984). These works have been further extended to incorporate the effect of third-order coupling between incident and reflected waves (Liu & Tsay 1984; Kirby 1986*b*). In particular, Kirby (1986*b*) used a Lagrangian formulation and derived new nonlinear coupling equations for a weakly nonlinear Stokes wave, which provided an effective and accurate model for both normal and oblique incidence conditions. The mild-slope-type equations are effective when the sandbar amplitude and its variation are mild, where series form solutions have been formulated for wave scattering problems as demonstrated by Liu, Li & Lin (2019), Liu & Zhou (2014) and Fang, Tang & Lin (2023). Recently, Liang *et al.* (2020) combined the mild-slope equation with the Mathieu instability theorem and derived a formula for phase downshift of Bragg resonance given the infinite bottom length condition. Alternatively, the Boussinesq equation, as an integral model, can be used to describe weak nonlinearity wave propagation over varying topography in shallow water (Madsen, Fuhrman & Wang 2005; Gao *et al.* 2021), while numerical solution is usually the only viable access.

To derive the analytical solutions for wave scattering over varying topography, not restricted to the shallow-water condition, Mei (1985) developed wave envelope equations based on the multiple-scale expansion to analyse Bragg scattering by sandbars. The equations and solutions were subsequently extended to oblique incidence (Mei *et al.* 1988; Kirby 1993), doubly sinusoidal ripples (Rey, Guazzelli & Mei 1996), including the current effect (Kirby 1988; Ardhuin & Magne 2007) and random waves with an irregular bottom (Ardhuin & Herbers 2002). Furthermore, the approach of Mei (1985) was further extended to linear Schrödinger equations by Hara & Mei (1988) to include higher-order effects of bottom and dispersion to investigate wave-envelope evolution. Although their equations have difficulties to propose exact solutions for incident and reflected wave amplitudes due to the introduction of additional boundary conditions for continuity of pressure, their analysis demonstrated the importance of the higher-order effects of the bottom and

dispersion on Bragg scattering. However, nonlinear wave interaction, which is known to be an influential factor that affects wave reflection by modifying wave speed and producing nonlinear behaviours, are difficult to express in the linear Schrödinger equations of Hara & Mei (1988).

The nonlinear Schrödinger (NLS) equation was initially designed for nonlinear waves propagation over a constant water depth (Benjamin & Feir 1967; Lake *et al.* 1977). In addition, the NLS has been extended to include wave–current or wave–wave interactions, as shown in Thomas, Kharif & Manna (2012) and Liao *et al.* (2017). In addition, Onorato, Osborne & Serio (2006) and Hammack, Henderson & Segur (2005) derived the coupled nonlinear Schrödinger (CNLS) equations for a two-wave system, providing the possibility to investigate the effects of nonlinear wave–wave interaction on Bragg scattering. Nevertheless, the NLS equation that directly incorporates all the higher-order bottom effects of sinusoidal sandbars, higher-order dispersion effects and wave nonlinearity, has not been reported yet, likely due to the increased complexity of introducing bottom undulations into two-progressive-wave interactions.

To include high-order effects induced by bottom, dispersion and the nonlinear wave interaction and to explore the underlying mechanisms of physical process of Bragg scattering, a new set of extended nonlinear Schrödinger (ENLS) equations is derived to describe wave scattering over periodic sinusoidal sandbars. This paper is organised as follows. In § 2, the multiple-scale expansion method is utilised to formulate a system of nonlinear equations that considers high-order bottom and dispersion effects, as well as the wave nonlinearity effect. In § 3, analytical solutions for the reflection and transmission rates of the linearised equations are constructed, presenting an analysis of the generation of the wave components, and their mathematical expression in the equations after carefully considering the complex interactions. Subsequently, the causes of the downshift behaviour are elucidated, and a theoretical formula for the downshift magnitude of the Bragg resonance is derived. In § 4, a numerical approach to the full ENLS equations is implemented to further examine the influence of the wave nonlinearity on the Bragg resonance.

2. Mathematical derivation

2.1. *Derivation of the coupled model*

In this section, the ENLS equations up to third order are derived to consider the additional high-order bottom, dispersion effects and nonlinear wave interactions on wave transformation over spatially periodic cosine sandbars. As depicted in figure 1, waves propagate over cosine sandbars with an averaged water depth of h below the mean water surface, with D and k_d representing the amplitude and wavenumber of sandbars, respectively. The bottom wavelength $\lambda_d = 2\pi/k_d$ is the spacing between adjacent peaks from a cosine topography. In addition, waves are assumed to be periodic in both time and space, with ω and k denoting the wave angular frequency and wavenumber. The waves are allowed to slowly modulate in both time and space scales during the propagation process.

Assuming the weak nonlinearity of waves and topography, we give priority to the problems over $[0, L]$, where the associated parameters, namely, the wave amplitude of incident waves and amplitude of sinusoidal sandbars, are characterised by the same small parameter ε. Here, we denote ϕ as the velocity potential function, which satisfies the Laplace equation in the fluid domain,

$$\frac{\partial^2 \phi}{\partial x^2} + \frac{\partial^2 \phi}{\partial z^2} = 0 \quad (-h + \sigma < z < \eta), \tag{2.1}$$
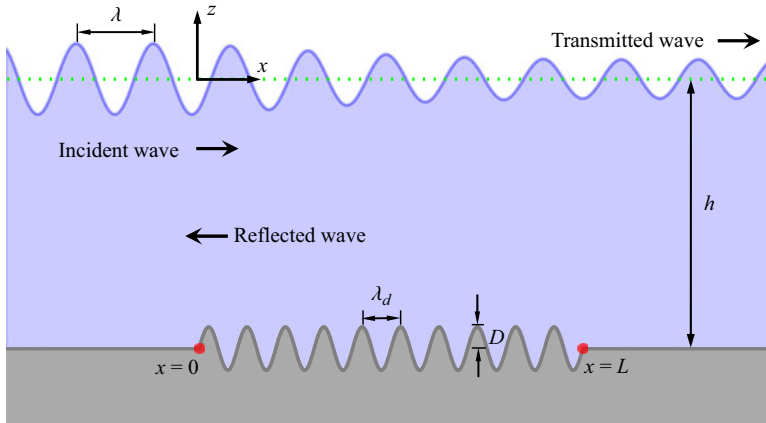
Figure 1. Schematic of the wave propagation domain.

where $\sigma = \sigma(x)$ and $\eta = \eta(x, t)$ are the bottom undulation above the mean bottom and free surface elevation, respectively. On the free surface, the kinematic and dynamic boundary conditions are

$$\frac{\partial \eta}{\partial t} + \frac{\partial \phi}{\partial x} \frac{\partial \eta}{\partial x} - \frac{\partial \phi}{\partial z} = 0 \quad (z = \eta), \tag{2.2}$$

and

$$\frac{\partial \phi}{\partial t} + g\eta + \frac{1}{2} \left[\left(\frac{\partial \phi}{\partial x} \right)^2 + \left(\frac{\partial \phi}{\partial z} \right)^2 \right] = 0 \quad (z = \eta). \tag{2.3}$$

Equations (2.2) and (2.3) are combined to give

$$\left(\frac{\partial}{\partial t} + \frac{\partial \eta}{\partial t} \frac{\partial}{\partial z} \right) \left\{ \frac{\partial \phi}{\partial t} + \frac{1}{2} \left[\left(\frac{\partial \phi}{\partial x} \right)^2 + \left(\frac{\partial \phi}{\partial z} \right)^2 \right] \right\} + g\phi_z - g\frac{\partial \phi}{\partial x} \frac{\partial \eta}{\partial x} = 0 \quad (z = \eta). \tag{2.4}$$

On the bottom, the no-flux boundary condition yields

$$\frac{\partial \phi}{\partial z} - \frac{\partial \phi}{\partial x} \frac{\partial \sigma}{\partial x} = 0 \quad (z = -h + \sigma). \tag{2.5}$$

To consider third-order effects on the Bragg resonance, the slow variables up to the second order are introduced to capture the higher-order effects of sinusoidal bottom and wave–wave interactions:

$$\xi_1 = \varepsilon x, \quad \xi_2 = \varepsilon^2 x, \quad \tau_1 = \varepsilon t, \quad \tau_2 = \varepsilon^2 t. \tag{2.6a–d}$$

The multiple-scale expansions for ϕ and η with third-order accuracy give

$$\phi = \varepsilon \phi_1 + \varepsilon^2 \phi_2 + \varepsilon^3 \phi_3 + O(\varepsilon^4) \tag{2.7}$$

and

$$\eta = \varepsilon \eta_1 + \varepsilon^2 \eta_2 + \varepsilon^3 \eta_3 + O(\varepsilon^4) \tag{2.8}$$

in which $\phi_1 = \phi_1(x, z, t, \xi_1, \tau_1, \xi_2, \tau_2)$, $\eta_1 = \eta_1(x, t, \xi_1, \tau_1, \xi_2, \tau_2)$, etc. Here $O(\ )$ is an infinitesimal of the same order. Notably, in comparison with the second-order analysis

979 A13-4

of Mei (1985), we utilise a third-order expansion and introduce two additional slow variables, ξ_2 and τ_2, to consider a third-order problem. In addition, we take into account the nonlinear effect in the surface boundary condition, accounting for wave–wave interactions and higher-order bottom and dispersion effects.

By substituting the solutions of (2.7) and (2.8) into (2.1) and utilising the boundary conditions of (2.3), (2.4) and (2.5) with Taylor series expansions at $z = 0$ (for (2.3) and (2.4)) and $z = -h$ (for (2.5)), boundary value problems (BVPs) can be obtained for each order of ε upon separation of the different orders.

2.1.1. *First-order problem*

The first-order problem is composed of waves propagating both forwards and backwards, as Mei (1985) demonstrated, and an additional non-propagative mode, B, which represents the wave-induced mean flow and is generated in the process of nonlinear wave modulations in slow spatial and time scales (Thomas *et al.* 2012). Considering the significant influence of term B on stability of wave modulation (Thomas *et al.* 2012; Francius & Kharif 2017; Dhar & Kirby 2023), wave kinematic and dynamic properties (Pizzo *et al.* 2023), and the geometry of the fluid particle trajectories (Wang, Guan & Vanden-Broeck 2020), we included this term in the present study.

Assuming the associated potential and surface elevation can be expressed as

$$\phi_1 = \left(\psi^+ A^+ S^+ + \psi^- A^- S^- + \text{c.c.} \right) + B, \tag{2.9}$$

and

$$\eta_1 = \tfrac{1}{2} A^+ S^+ + \tfrac{1}{2} A^- S^- + \text{c.c.}, \tag{2.10}$$

where c.c. denotes the conjugate component. The superscripts $+$ and $-$ refer to the incident and reflected waves, respectively. Here $\psi^\pm$ are the corresponding vertical profiles,

$$\psi^\pm = -\frac{g\mathrm{i}}{2\omega} \frac{\cosh k(z+h)}{\cosh kh}. \tag{2.11}$$

We use A^+ and A^- to denote the complex wave amplitudes, and B is a function, modulated by the slow variables,

$$A^\pm = A^\pm \left(\xi_1, \tau_1, \xi_2, \tau_2 \right), \quad B^\pm = B^\pm \left(\xi_1, \tau_1, \xi_2, \tau_2 \right). \tag{2.12a,b}$$

Here S^+ and S^- are functions of phases,

$$S^\pm = \exp(\pm \mathrm{i}kx - \mathrm{i}\omega t). \tag{2.13}$$

We use ω to denote the angular frequency that satisfies the dispersion equation, $\omega = gk \tanh kh$, while the wavenumber k should satisfy the standard Bragg resonance condition established by Mei (1985) to accurately capture wave reflection in the vicinity of the resonance,

$$k = \tfrac{1}{2} k_d. \tag{2.14}$$

Thus, the cosine topography can be expressed in terms of the wavenumber k

$$\sigma = D \cos 2kx. \tag{2.15}$$

2.1.2. *Second-order problem*

At $O(\varepsilon^2)$, the BVP can be represented by the following system of equations

$$\frac{\partial^2 \phi_2}{\partial x^2} + \frac{\partial^2 \phi_2}{\partial z^2} = T_2 \quad (-h < z < 0), \tag{2.16}$$

$$\frac{\partial^2 \phi_2}{\partial t^2} + g\frac{\partial \phi_2}{\partial z} = P_2 \quad (z = 0), \tag{2.17}$$

$$\frac{\partial \phi_2}{\partial z} = W_2 \quad (z = -h), \tag{2.18}$$

$$\eta_2 = R_2 \quad (z = 0), \tag{2.19}$$

where T_2, P_2, W_2 and R_2 are compulsory components consisting of lower-order terms, which can be expressed as follows:

$$
\left.\begin{aligned}
T_2 &= -2\frac{\partial^2 \phi_1}{\partial x \partial \xi_1} = -\frac{gk}{\omega}\frac{\cosh k(z+h)}{\cosh kh}\left(\frac{\partial A^+}{\partial \xi_1}S^+ - \frac{\partial A^-}{\partial \xi_1}S^-\right) + \text{c.c.},\\[6pt]
P_2 &= \left(-2\frac{\partial^2 \phi_1}{\partial t \partial \tau_1} - \frac{\partial \eta_1}{\partial t}\frac{\partial^2 \phi_1}{\partial z \partial t} - \frac{\partial \phi_1}{\partial z}\frac{\partial^2 \phi_1}{\partial z \partial t} - \eta_1\frac{\partial^3 \phi_1}{\partial z \partial t^2} - g\eta_1\frac{\partial^2 \phi_1}{\partial z^2} + g\frac{\partial \eta_1}{\partial x}\frac{\partial \phi_1}{\partial x} - \frac{\partial \phi_1}{\partial x}\frac{\partial^2 \phi_1}{\partial x \partial t}\right)\Bigg|_{z=0}\\[6pt]
&= g\left(\frac{\partial A^+}{\partial \tau_1}S^+ + \frac{\partial A^-}{\partial \tau_1}S^-\right) - \frac{\mathrm{i}\left(3\omega^4 + g^2k^2\right)}{2\omega}A^+A^-S_{0,2}^+\\[6pt]
&\quad - \frac{3\mathrm{i}\left(\omega^4 - g^2k^2\right)}{4\omega}\left[\left(A^+\right)^2 S_{2,2}^+ + \left(A^-\right)^2 S_{2,2}^-\right] + \text{c.c.},\\[6pt]
W_2 &= -\sigma\frac{\partial^2 \phi_1}{\partial z^2}\Bigg|_{z=-h} + \frac{\mathrm{d}\sigma}{\mathrm{d}x}\frac{\partial \phi_1}{\partial x}\Bigg|_{z=-h}\\[6pt]
&= -\frac{\mathrm{i}Dgk^2}{4\omega\cosh kh}\left(A^-S^+ + A^+S^-\right) + \frac{3\mathrm{i}Dgk^2}{4\omega\cosh kh}\left(A^+S_{3,1}^+ + A^-S_{3,1}^-\right) + \text{c.c.},\\[6pt]
R_2 &= -\frac{1}{g}\left\{\frac{\partial \phi_2}{\partial t} + \frac{\partial \phi_1}{\partial \tau_1} + \eta_1\frac{\partial^2 \phi_1}{\partial z \partial t} + \frac{1}{2}\left[\left(\frac{\partial \phi_1}{\partial x}\right)^2 + \left(\frac{\partial \phi_1}{\partial z}\right)^2\right]\right\}\\[6pt]
&= \frac{\omega^4 - g^2k^2}{4g\omega^2}\left[A^+\left(A^+\right)^* + A^-\left(A^-\right)^*\right] - \frac{1}{g}\frac{\partial B}{\partial \tau_1} - \frac{1}{g}\frac{\partial \phi_2}{\partial t}\Bigg|_{z=0}\\[6pt]
&\quad + \left[\frac{\mathrm{i}}{2\omega}\left(\frac{\partial A^+}{\partial \tau_1}S_{1,1}^+ + \frac{\partial A^-}{\partial \tau_1}S_{1,1}^-\right) + \frac{3\omega^4 + g^2k^2}{4g\omega^2}A^+A^-S_{0,2}^+ + \frac{\omega^4 + g^2k^2}{4g\omega^2}A^+\left(A^-\right)^* S_{2,0}^+\right.\\[6pt]
&\quad \left. + \frac{3\omega^4 - g^2k^2}{8g\omega^2}\left(A^+\right)^2 S_{2,2}^+ + \frac{3\omega^4 - g^2k^2}{8g\omega^2}\left(A^-\right)^2 S_{2,2}^- + \text{c.c.}\right],
\end{aligned}\right\} \tag{2.20}
$$

in which $S_{m,n}^+$ and $S_{m,n}^-$ denote the phase functions for waves propagating in the forward and backward directions, expressed as

$$S_{m,n}^{\pm} = \exp(\mathrm{i}(\pm mkx - n\omega t)), \tag{2.21}$$

in particular, $S^{\pm} = S_{1,1}^{\pm}$. By solving (2.16)–(2.18) (detailed in Appendix A), ϕ_2 can be expressed as

$$
\phi_2 = -\frac{g \sinh k(z+h)}{4\omega \cosh kh} \left[2(z+h) \left(\frac{\partial A^+}{\partial \xi_1} S_{1,1}^+ - \frac{\partial A^-}{\partial \xi_1} S_{1,1}^- \right) + \mathrm{i}kD \left(A^- S_{1,1}^+ + A^+ S_{1,1}^- \right) \right]
$$
$$
- \frac{3\mathrm{i} \left(\omega^4 - g^2 k^2 \right)^2}{16\omega^7 \operatorname{sech} 2k(z+h)} \left[\left(A^+ \right)^2 S_{2,2}^+ + \left(A^- \right)^2 S_{2,2}^- \right] + \frac{\mathrm{i} \left(3\omega^4 + g^2 k^2 \right)}{8\omega^3} A^+ A^- S_{0,2}^+
$$
$$
+ \frac{\mathrm{i}Dgk}{4\omega \cosh kh} \frac{3gk \cosh 3kz + \omega^2 \sinh 3kz}{\omega^2 \cosh 3kh - 3gk \sinh 3kh} \left(A^+ S_{3,1}^+ + A^- S_{3,1}^- \right) + \text{c.c.} \tag{2.22}
$$

Then, from (2.19), η_2 can be derived,

$$
\eta_2 = \frac{\omega^4 + g^2 k^2}{4g\omega^2} \left[A^+ \left(A^+ \right)^* + A^- \left(A^- \right)^* \right] - \frac{1}{g} \frac{\partial B}{\partial \tau_1} + \left\{ \frac{3D \left(\omega^4 - g^2 k^2 \right)^2}{32g^3 k^2 \omega^2} \left(A^+ S_{3,1}^+ + A^- S_{3,1}^- \right) \right.
$$
$$
+ \frac{1}{4gk\omega} \left[2\mathrm{i} \left(gk \frac{\partial A^+}{\partial \tau_1} - h\omega^3 \frac{\partial A^+}{\partial \xi_1} \right) + Dk\omega^3 A^- \right] S_{1,1}^+
$$
$$
+ \frac{1}{4gk\omega} \left[2\mathrm{i} \left(gk \frac{\partial A^-}{\partial \tau_1} + h\omega^3 \frac{\partial A^-}{\partial \xi_1} \right) + Dk\omega^3 A^+ \right] S_{1,1}^-
$$
$$
\left. - \frac{gk^2 \left(\omega^4 - 3g^2 k^2 \right)}{8\omega^6} \left[\left(A^+ \right)^2 S_{2,2}^+ + \left(A^- \right)^2 S_{2,2}^- \right] + \frac{\omega^4 + g^2 k^2}{4g\omega^2} A^+ \left(A^- \right)^* S_{2,0}^+ + \text{c.c.} \right\}. \tag{2.23}
$$

As demonstrated in Appendix A, the following solvable conditions must be satisfied:

$$
\int_{-h}^{0} \left(\mp \frac{gk}{\omega} \frac{\cosh k(z+h)}{\cosh kh} \frac{\partial A^{\pm}}{\partial \xi_1} \right) \psi^{\pm} \, \mathrm{d}z = \left(\frac{\partial A^{\pm}}{\partial \tau_1} \right) \psi^{\pm} \Big|_{z=0} - \left(-\frac{\mathrm{i}Dgk^2}{4\omega \cosh kh} A^{\mp} \right) \psi^{\pm} \Big|_{z=-h} \tag{2.24}
$$

which can be simplified as

$$
\frac{\partial A^{\pm}}{\partial \tau_1} + C_g^{\pm} \frac{\partial A^{\pm}}{\partial \xi_1} + \mathrm{i}D_0^{\pm} A^{\mp} = 0 \tag{2.25}
$$

in which $C_g^{\pm}$ and $D_0^{\pm}$ are the group velocities and topography-induced terms,

$$
C_g^{\pm} = \pm \left(\frac{\omega}{2k} + h\omega \operatorname{csch} 2kh \right), \tag{2.26}
$$

and

$$
D_0^{\pm} = \tfrac{1}{2} Dk\omega \operatorname{csch} 2kh. \tag{2.27}
$$

in which $D_0^{\pm}$, with the dimension of frequency, is a forcing term and represents leading-order interaction between the waves and the sandbars, where the forward (backward) mode is reflected by the ripple components, thereby forcing a resonant backward (forward) wave mode. Its expression is identical to earlier work (Mei 1985) for pure wave condition. If we ignore the current effects in the early work of Kirby (1988), the present expressions of $D_0^{\pm}$ in (2.27) are identical to their results.

2.1.3. *Third-order problem*

For the third-order problem, the solvable conditions of the singular modes, $S_{1,1}^+$ and $S_{1,1}^-$, and the zero mode are considered in the present solution. The other harmonics in the compulsory terms, which have no association with resonance, are not considered here. The third-order problem for potential function is defined as

$$
\left.
\begin{aligned}
\frac{\partial^2 \phi_3}{\partial x^2} + \frac{\partial^2 \phi_3}{\partial z^2} &= T_{0,0}^{3,+} + \left(T_{1,1}^{3,+} S_{1,1}^+ + T_{1,1}^{3,-} S_{1,1}^- + \text{c.c.} \right) \quad (-h < z < 0), \\
\frac{\partial^2 \phi_3}{\partial t^2} + g \frac{\partial \phi_3}{\partial z} &= P_{0,0}^{3,+} + \left(P_{1,1}^{3,+} S_{1,1}^+ + P_{1,1}^{3,-} S_{1,1}^- + \text{c.c.} \right) \quad (z = 0), \\
\frac{\partial \phi_3}{\partial z} &= W_{1,1}^{3,+} S_{1,1}^+ + W_{1,1}^{3,-} S_{1,1}^- + \text{c.c.} \quad (z = -h),
\end{aligned}
\right\}
\tag{2.28}
$$

in which

$$
\left.
\begin{aligned}
T_{0,0}^{3,+} &= -\frac{\partial^2 B}{\partial \xi_1^2}, \\
T_{1,1}^{3,\pm} &= \mp \frac{g \operatorname{sech} kh}{2\omega} \left\{ 2k \cosh k(z+h) \frac{\partial A^\pm}{\partial \xi_2} + Dk^2 \sinh k(z+h) \frac{\partial A^\mp}{\partial \xi_1} \right. \\
&\qquad\qquad \left. \mp \mathrm{i}[2k(z+h)\sinh k(z+h) + \cosh k(z+h)] \frac{\partial^2 A^\pm}{\partial \xi_1^2} \right\}, \\
P_{0,0}^{3,+} &= \frac{\omega^4 - g^2 k^2}{4\omega^2} \frac{\partial \left[A^+ \left(A^+\right)^* + A^- \left(A^-\right)^* \right]}{\partial \tau_1} + \frac{g^2 k}{2\omega} \frac{\partial \left[A^+ \left(A^+\right)^* - A^- \left(A^-\right)^* \right]}{\partial \xi_1} - \frac{\partial^2 B}{\partial \tau_1^2}, \\
P_{1,1}^{3,\pm} &= g \frac{\partial A^\pm}{\partial \tau_2} + \frac{\mathrm{i}g}{2\omega} \frac{\partial^2 A^\pm}{\partial \tau_1^2} \mp \frac{\mathrm{i}h\omega^2}{k} \frac{\partial^2 A^\pm}{\partial \xi_1 \partial \tau_1} + \frac{\omega^2 D}{2} \frac{\partial A^\mp}{\partial \tau_1} - \frac{\mathrm{i} \left(\omega^4 + g^2 k^2\right)^2}{4g\omega^3} A^\pm A^\mp \left(A^\mp\right)^* \\
&\quad + \frac{\mathrm{i} \left(9g^6 k^6 - 12g^4 k^4 \omega^4 + 13g^2 k^2 \omega^8 - 2\omega^{12}\right)}{16g\omega^7} \left(A^\pm\right)^2 \left(A^\pm\right)^* \\
&\quad + \frac{\mathrm{i} \left(\omega^4 - g^2 k^2\right)}{2g\omega} A^\pm \frac{\partial B}{\partial \tau_1} \pm \mathrm{i}gk A^\pm \frac{\partial B}{\partial \xi_1}, \\
W_{1,1}^{3,\pm} &= \frac{3\mathrm{i}D^2 g k^3 \operatorname{sech} kh \left(3gk \cosh 3kh - \omega^2 \sinh 3kh\right)}{24 gk\omega \sinh 3kh - 8\omega^3 \cosh 3kh} A^\pm.
\end{aligned}
\right\}
\tag{2.29}
$$

At the order of ε^3, (A25) yields solvability conditions for singular components, $S_{1,1}^\pm$, by way of the Green formula depicted in (A24)

$$
\int_{-h}^0 T_{1,1}^{3,\pm} \psi^\pm \, \mathrm{d}z = \frac{1}{g} P_{1,1}^{3,\pm} \left. \psi^\pm \right|_{z=0} - W_{1,1}^{3,\pm} \left. \psi^\pm \right|_{z=-h},
\tag{2.30}
$$

which can be further integrated with the substitution of $T_{1,1}^{3,\pm}$, etc., resulting in two coupled equations for A^+, A^- and B

$$
\frac{\partial A^\pm}{\partial \tau_2} + C_g^\pm \frac{\partial A^\pm}{\partial \xi_2} + B_1^\pm \frac{\partial^2 A^\pm}{\partial \tau_1^2} + B_2^\pm \frac{\partial^2 A^\pm}{\partial \xi_1 \partial \tau_1} + B_3^\pm \frac{\partial^2 A^\pm}{\partial \xi_1^2} + D_1^\pm \frac{\partial A^\mp}{\partial \tau_1} + D_2^\pm \frac{\partial A^\mp}{\partial \xi_1}
$$
$$
+ D_3^\pm A^\pm + \left\{ \sigma_1^\pm \left|A^\pm\right|^2 + \sigma_2^\pm \left|A^\mp\right|^2 + \sigma_3^\pm \frac{\partial B}{\partial \tau_1} + \sigma_4^\pm \frac{\partial B}{\partial \xi_1} \right\} A^\pm = 0,
\tag{2.31}
$$

in which $|A^\pm|$ corresponds the modulus of $A^\pm$, given by $\sqrt{A^\pm (A^\pm)^*}$. The coefficients can be expressed as

$$
\left.
\begin{aligned}
B_1^\pm &= \frac{i}{2\omega}, B_2^\pm = \mp ih \tanh kh, B_3^\pm = -\frac{ih\omega}{2k} \coth kh, D_1^\pm = \frac{D\omega^2}{2g}, D_2^\pm = \pm \frac{D\omega^3}{4gk}, \\
D_3^\pm &= \frac{3gk \cosh 3kh - \omega^2 \sinh 3kh}{4\omega^2 \cosh 3kh - 12gk \sinh 3kh} \frac{3iD^2 k^2 \omega}{\sinh 2kh}, \\
\sigma_1^\pm &= \frac{igk^3 (20 + 13 \cosh 2kh + 2 \cosh 4kh + \cosh 6kh)}{8\omega \sinh^3 2kh}, \\
\sigma_2^\pm &= -\frac{i\left(\omega^4 + g^2 k^2\right)^2}{4g^2 \omega^3}, \sigma_3^\pm = \frac{i\left(\omega^4 - g^2 k^2\right)}{2g^2 \omega}, \sigma_4^\pm = \pm ik.
\end{aligned}
\right\}
\tag{2.32}
$$

The zero mode, $T_{0,0}^{3,+}$, does not depend on z. Consequently, combining the Laplace equation, bottom boundary and bottom conditions, the solvable condition for B is derived to fulfil the surface boundary condition,

$$
gh T_{0,0}^{3,+} = P_{0,0}^{3,+}.
\tag{2.33}
$$

By introducing the expressions of $T_{0,0}^{3,+}$, etc., (2.33) is transformed into a hyperbolic partial differential equation

$$
\frac{\partial^2 B}{\partial \tau_1^2} - gh \frac{\partial^2 B}{\partial \xi_1^2} = \frac{\omega^4 - g^2 k^2}{4\omega^2} \frac{\partial \left(|A^+|^2 + |A^-|^2\right)}{\partial \tau_1} + \frac{g^2 k}{2\omega} \frac{\partial \left(|A^+|^2 - |A^-|^2\right)}{\partial \xi_1}.
\tag{2.34}
$$

We multiply (2.25) by $(A^\pm)^*$ and, upon conjugation and summation, obtain

$$
\frac{\partial \left(|A^+|^2 + |A^-|^2\right)}{\partial \tau_1} + C_g^+ \frac{\partial \left(|A^+|^2 - |A^-|^2\right)}{\partial \xi_1} = 0,
\tag{2.35}
$$

which indicates that (2.34) can be automatically satisfied by constructing the formulation of

$$
\frac{\partial B}{\partial \tau_1} = -C_g^+ \lambda \left(|A^+|^2 + |A^-|^2\right), \quad \frac{\partial B}{\partial \xi_1} = \lambda \left(|A^+|^2 - |A^-|^2\right),
\tag{2.36a,b}
$$

in which

$$
\lambda = \frac{1}{C_g^{+2} - gh} \left(\frac{g^2 k}{2\omega} - C_g^+ \frac{\omega^4 - g^2 k}{4\omega^2}\right).
\tag{2.37}
$$

By introducing the first-order derivatives of B from (2.36a,b) into (2.31), we can eliminate the terms related to it and thereby attain the second set of solvability conditions for $A^\pm$

$$
\frac{\partial A^\pm}{\partial \tau_2} + C_g^\pm \frac{\partial A^\pm}{\partial \xi_2} + B_1^\pm \frac{\partial^2 A^\pm}{\partial \tau_1^2} + B_2^\pm \frac{\partial^2 A^\pm}{\partial \xi_1 \partial \tau_1} + B_3^\pm \frac{\partial^2 A^\pm}{\partial \xi_1^2} + D_1^\pm \frac{\partial A^\mp}{\partial \tau_1}
$$

$$
+ D_2^\pm \frac{\partial A^\mp}{\partial \xi_1} + D_3^\pm A^\pm + \left\{F_1^\pm |A^\pm|^2 + F_2^\pm |A^\mp|^2\right\} A^\pm = 0,
\tag{2.38}
$$

in which

$$
\left.
\begin{aligned}
F_1^\pm &= \frac{\mathrm{i}gk^3(20 + 13\cosh 2kh + 2\cosh 4kh + \cosh 6kh)}{8\omega \sinh^3 2kh} - \frac{\mathrm{i}\left[2g^2k\omega + C_g^+\left(g^2k^2 - \omega^4\right)\right]^2}{8g^2\omega^3\left[gh - C_g^{+2}\right]}, \\
F_2^\pm &= -\frac{\mathrm{i}\left(\omega^4 + g^2k^2\right)^2}{4g^2\omega^3} - \frac{\mathrm{i}\left[-4g^4k^2\omega^2 + \left(\omega^4 - g^2k^2\right)^2 C_g^{+2}\right]}{8g^2\omega^3\left[gh - C_g^{+2}\right]}.
\end{aligned}
\right\}
\tag{2.39}
$$

Equation (2.38) can be reduced to the linear Schrödinger equation derived by Hara & Mei (1988), if wave–wave interaction is neglected and the transformations to (2.25) are implemented. However, their equation formulates a partial differential equation with respect to the second-order derivative of the spatial variable x, necessitating additional boundary conditions for continuity of pressure, thereby posing a challenge for seeking exact solutions. Therefore, they derived the ratio of the envelope height at antinodes in the strip to the envelope height at the strip's edge to settle for the second best. In the present study, to directly identify the solutions for incident and reflected wave evolutions, the differential transformations on (2.25) are employed to replace the second derivatives with respect to x in (2.38) as follows:

$$
\left.
\begin{aligned}
\frac{\partial^2 A^\pm}{\partial \xi_1^2} &\rightarrow -\frac{\mathrm{i}D_0^\pm}{C_g^\pm}\frac{\partial A^\mp}{\partial \xi_1} - \frac{1}{C_g^\pm}\frac{\partial^2 A^\pm}{\partial \tau_1 \partial \xi_1}, \\
\frac{\partial^2 A^\pm}{\partial \tau_1 \partial \xi_1} &\rightarrow -\frac{\mathrm{i}D_0^\pm}{C_g^\pm}\frac{\partial A^\mp}{\partial \tau_1} - \frac{1}{C_g^\pm}\frac{\partial^2 A^\pm}{\partial \tau_1^2}.
\end{aligned}
\right\}
\tag{2.40}
$$

We introduce transforms of temporal and spatial scales to recover x and t

$$
\varepsilon\frac{\partial}{\partial \tau_1} + \varepsilon^2\frac{\partial}{\partial \tau_2} \rightarrow \frac{\partial}{\partial t}, \quad \varepsilon\frac{\partial}{\partial \xi_1} + \varepsilon^2\frac{\partial}{\partial \xi_2} \rightarrow \frac{\partial}{\partial x},
\tag{2.41a,b}
$$

which enables $A^\pm(\xi_1, \tau_1, \xi_2, \tau_2)$ to return to $A^\pm(x, t)$ and, thus, obtain a set of coupled nonlinear equations for A^+ and A^-, which can be employed to investigate the envelope evolution of waves,

$$
\frac{\partial A^+}{\partial t} + C_g^+\frac{\partial A^+}{\partial x} + \mathrm{i}D_0^+ A^-
$$

$$
+ \overbrace{\left(D_1^+ - \frac{\mathrm{i}B_2^+ D_0^+}{C_g^+} + \frac{\mathrm{i}B_3^+ D_0^+}{\left(C_g^+\right)^2}\right)\frac{\partial A^-}{\partial t} + \left(D_2^+ - \frac{\mathrm{i}B_3^+ D_0^+}{C_g^+}\right)\frac{\partial A^-}{\partial x} + D_3^+ A^+}^{\text{high-order bottom effect}}
$$

$$
+ \underbrace{\left(B_1^+ - \frac{B_2^+}{C_g^+} + \frac{B_3^+}{\left(C_g^+\right)^2}\right)\frac{\partial^2 A^+}{\partial t^2}}_{\text{high-order dispersion effect}} + \underbrace{F_1^+\left|A^+\right|^2 A^+ + F_2^+\left|A^-\right|^2 A^+}_{\text{nonlinear wave interaction}} = 0,
\tag{2.42}
$$

$$\frac{\partial A^-}{\partial t} + C_g^- \frac{\partial A^-}{\partial x} + \mathrm{i} D_0^- A^+$$

$$\overbrace{+ \left(D_1^- - \frac{\mathrm{i} B_2^- D_0^-}{C_g^-} + \frac{\mathrm{i} B_3^- D_0^-}{\left(C_g^- \right)^2} \right) \frac{\partial A^+}{\partial t} + \left(D_2^- - \frac{\mathrm{i} B_3^- D_0^-}{C_g^-} \right) \frac{\partial A^+}{\partial x} + D_3^- A^-}^{\text{high-order bottom effect}}$$

$$\underbrace{+ \left(B_1^- - \frac{B_2^-}{C_g^-} + \frac{B_3^-}{\left(C_g^- \right)^2} \right) \frac{\partial^2 A^-}{\partial t^2}}_{\text{high-order dispersion effect}} + \underbrace{F_1^- \left| A^- \right|^2 A^- + F_2^- \left| A^+ \right|^2 A^-}_{\text{nonlinear wave interaction}} = 0. \quad (2.43)$$

Equations (2.42) and (2.43) are the newly derived ENLS equations, consisting of the basic governing equations of Mei (1985) (the first three items), the bottom effect terms with $D_0^\pm$ representing the first-order bottom effect and $D_1^\pm$, $D_2^\pm$ and $D_3^\pm$ being second-order bottom effects, the high-order wave dispersion effect terms ($B_1^\pm$, etc.) and the nonlinear terms with $F_1^\pm$ and $F_2^\pm$ related to the wave–wave interactions.

The internal correlations between the newly derived ENLS and the Schrödinger equations are summarised as follows. (1) If the topography-related terms are eliminated and the substitution of $\partial^2/\partial t^2$ for $\partial^2/\partial x \partial t$ and $\partial^2/\partial x^2$ is applied in accordance with the first solvable conditions, the ENLS is reduced to a range of variants of the Schrödinger equation. (2) If the sandbars vanish and water depth is assumed to be infinite, the ENLS can be reduced to the CNLS equations established by Hammack *et al.* (2005); compared with the CNLS of Onorato *et al.* (2006), the only slight difference lies on the coefficients $F_2^\pm$. (3) The ENLS can be simplified to the NLS equations of Thomas *et al.* (2012) and Liao *et al.* (2017) if the influence of the current is neglected.

3. Exact solution for the linearised ENLS equations

3.1. *Derivation of the exact solution*

Closed-form solutions for the ENLS equations are difficult to propose due to the nonlinearity derived from the wave–wave interactions. However, by assuming wave amplitudes to be sufficiently small, the equations can be reduced to a linear system coupling A^+ and A^-, leading to exact solutions, which enables systematic investigation on the influence of topographical factors on Bragg resonance. Therefore, in this section, by neglecting the wave nonlinearity, the linearised ENLS equations are obtained

$$\frac{\partial A^+}{\partial t} + C_g^+ \frac{\partial A^+}{\partial x} + \mathrm{i} D_0^+ A^- + \left(B_1^+ - \frac{B_2^+}{C_g^+} + \frac{B_3^+}{(C_g^+)^2} \right) \frac{\partial^2 A^+}{\partial t^2}$$

$$+ \left(D_1^+ - \frac{\mathrm{i} B_2^+ D_0^+}{C_g^+} + \frac{\mathrm{i} B_3^+ D_0^+}{(C_g^+)^2} \right) \frac{\partial A^-}{\partial t} + \left(D_2^+ - \frac{\mathrm{i} B_3^+ D_0^+}{C_g^+} \right) \frac{\partial A^-}{\partial x} + D_3^+ A^+ = 0, \quad (3.1)$$

$$\frac{\partial A^-}{\partial t} + C_g^- \frac{\partial A^-}{\partial x} + \mathrm{i} D_0^- A^+ + \left(B_1^- - \frac{B_2^-}{C_g^-} + \frac{B_3^-}{(C_g^-)^2} \right) \frac{\partial^2 A^-}{\partial t^2}$$

$$+ \left(D_1^- - \frac{\mathrm{i} B_2^- D_0^-}{C_g^-} + \frac{\mathrm{i} B_3^- D_0^-}{(C_g^-)^2} \right) \frac{\partial A^+}{\partial t} + \left(D_2^- - \frac{\mathrm{i} B_3^- D_0^-}{C_g^-} \right) \frac{\partial A^+}{\partial x} + D_3^- A^- = 0. \quad (3.2)$$

As illustrated in figure 1, an incident wave train of both temporally and spatially periodic waves arrives from $x = -\infty$ and these waves are continuously reflected by the bottom sandbars, forming reflected waves that propagate in the reverse direction and produce standing waves by the superposition of the incident and reflected waves. In the region $x > L$, where the varying topography vanishes, only the forward-propagating mode exists, designated as transmitted waves. The region $0 < x < L$ is highlighted by periodic sinusoidal bars of amplitude D and wavenumber $2k$, and L is the total length of the sandbars and $N_d = L/\lambda_d$ denotes the number of sandbars.

Let the incident and reflected waves be slightly detuned from the Bragg resonance, with their wave frequencies being $\omega^+ = \omega^- = \omega + \omega'$, where ω' implies wavenumber deviations k' and k'' for the incident and reflected waves, respectively. Over the sandbars $0 < x < L$, we can find solutions such as

$$A^+ = A_0 T(x) e^{-i\omega' t} \quad (0 < x < L), \tag{3.3}$$

and

$$A^- = A_0 R(x) e^{-i\omega' t} \quad (0 < x < L). \tag{3.4}$$

Let $\tilde{R}$ denote the reflection coefficient, given by $|R(0)|$. An exact solution for the reflection rate, $\tilde{R}$, can be written as (details can be found in Appendix B)

$$\tilde{R} = \sqrt{\frac{Q_1^2}{|P \cot PL|^2 + Q_2^2}}, \tag{3.5}$$

in which Q_1, Q_2 and P are functions of ω':

$$
\left.
\begin{aligned}
Q_1 &= \frac{-i\left\{E_3\left[D_3^+ + \omega'\left(-i + E_2\omega'\right)\right] + C_g^+\left(E_1\omega' + iD_0^+\right)\right\}}{E_3^2 - \left(C_g^+\right)^2}, \\[2mm]
Q_2 &= \frac{E_3 D_0^+ - i\left\{E_1 E_3 \omega' + C_g^+\left[D_3^+ + \omega'\left(-i + E_2\omega'\right)\right]\right\}}{E_3^2 - \left(C_g^+\right)^2}, \\[2mm]
P &= \sqrt{\frac{\left(D_3^+ + \omega'\left(-i + E_2\omega'\right)\right)^2 - \left(E_1\omega' + iD_0^+\right)^2}{E_3^2 - \left(C_g^+\right)^2}},
\end{aligned}
\right\} \tag{3.6}
$$

where E_1, E_2 and E_3 are coefficients, expressed as

$$
\left.
\begin{aligned}
E_1 &= -\frac{iD\left(g^4 h k^4 + g\omega^6 - h\omega^8\right)}{2\left(g^2 h k^2 + g\omega^2 - h\omega^4\right)^2}, \\[2mm]
E_2 &= -\frac{i}{2\omega} + 2ih\omega \frac{\left(-g + h\omega^2\right)\left(-g^2 k^2 + \omega^4\right)}{\left(g^2 h k^2 + g\omega^2 - h\omega^4\right)^2}, \\[2mm]
E_3 &= D\left(-\frac{gk}{4\omega} + \frac{\omega^3}{4gk} + \frac{g^2 k\omega}{4g^2 h k^2 + 4g\omega^2 - 4h\omega^4}\right).
\end{aligned}
\right\} \tag{3.7}
$$

It is clear that the only difference between the present solution (3.5) and the solution of Mei (1985) lies in the terms Q_1, Q_2 and P. If the higher-order contributions of E_1, E_2, E_3

979 A13-12

Case	h (m)	D/h	k_d (m^{-1})	λ_d (m)	N_d	L (m)
D1	0.312	0.160	2π	1.0	10	10
L1	0.220	0.159	4π	0.5	10	5

Table 1. Parameters for wave scattering by sinusoidal sandbars.

and D_3^+ are set to zero, the present solution reduces to the solution of Mei (1985),

$$\tilde{R}_M = \sqrt{\frac{Q_{1,M}^2}{Q_{2,M}^2 + |P_M \cot P_M L|^2}}, \tag{3.8}$$

in which

$$Q_{1,M} = -\frac{D_0^+}{C_g^+}, \quad Q_{2,M} = \frac{\omega'}{C_g^+}, \quad P_M = \frac{1}{C_g^+}\sqrt{(\omega')^2 - (D_0^+)^2}, \tag{3.9a–c}$$

where the subscript M represents the solution of Mei (1985). $Q_{1,M}$, $Q_{2,M}$ and P_M are even functions with respect to ω', indicating good symmetry with $\tilde{R}_M(\omega') = \tilde{R}_M(-\omega')$ and the maximum reflection occurring at $\omega' = 0$. However, as evidenced by the inequalities of $Q_1(\omega') \neq Q_1(-\omega')$, $Q_2(\omega') \neq Q_2(-\omega')$ and $P(\omega') \neq P(-\omega')$, the present solution is not symmetrically distributed, which could potentially shift the positions of maximum reflection.

3.2. *Verifications of the solution for reflection*

To verify the analytical solution for reflection in (3.5), experiment-based wave scattering by sinusoidal sandbars is investigated. The geometrical configuration of the experimental set-up is depicted in figure 1. The performance of the present solution is verified by comparing it with the experiments conducted by Davies & Heathershaw (1984) and Laffitte *et al.* (2021), denoted as D1 and L1, respectively. The wave- and topographic-related parameters of the experiments are shown in table 1.

Figure 2 shows the comparisons of the reflection $\tilde{R}$ obtained from the present solution, the analytical solution from Mei (1985), the numerical solution of Liu & Yue (1998), and the measured data by Davies & Heathershaw (1984) and Laffitte *et al.* (2021). The red dotted lines in figure 2(a) signify $2k^+/k_d = 1$, which is the peak of the Bragg resonance predicted by Mei (1985). However, in practice, a slight phase downshift is commonly observed, as indicated by the numerical solutions of Liu & Yue (1998) and the measured data, which is accurately captured by the present solution. In prior research studies, the downshift characteristics for case D1 were investigated (Madsen *et al.* 2005; Liang *et al.* 2020), and the results of these studies are summarised in table 2.

Table 2 presents the results of the wavenumber and reflection rate for case D1. As can be observed, based on and extending the pioneering work of Mei (1985), the present analytical solution can accurately describe the downshift behaviour of Bragg resonance and precisely capture the shift magnitude of the peak Bragg resonance phase.

While the phenomenon of the downshift of the wave frequency upon resonance has been extensively reported, providing essential parameters for the design of artificial bars for coastal protection, the underlying mechanism for its formation remains elusive. Therefore, it is of great significance to elucidate the mechanism of the downshift behaviour and
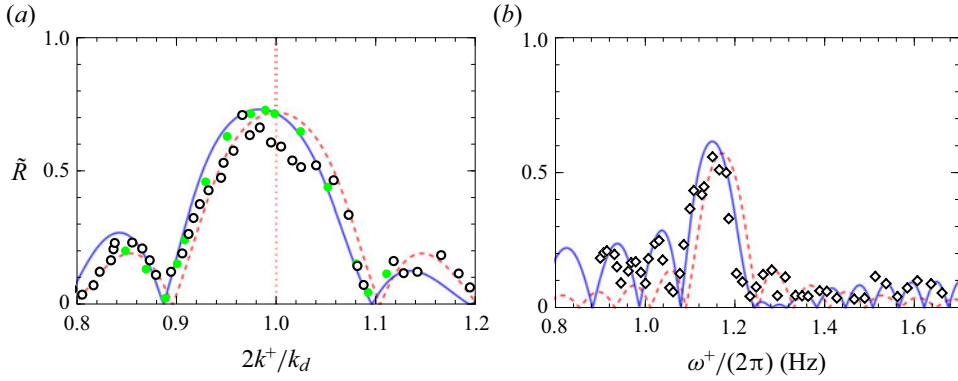
Figure 2. Comparison of the reflection rate $\tilde{R}$ for case-D1 and case-L1 among the present solution in (3.5) (blue solid line), analytical solution from Mei (1985) in (3.8) (red dashed line), numerical solutions of Liu & Yue (1998) (green dots) and experimental data from Davies & Heathershaw (1984) (black circles) and Laffitte *et al.* (2021) (black diamond), respectively. (*a*) case D1; (*b*) case L1.

Variables	The present solution	Liu & Yue (1998)	Madsen *et al.* (2005)	Liang *et al.* (2020)	Mei (1985)
$2k^+/k_d$	0.983	0.989	0.980	0.991	1
$\tilde{R}$	0.731	0.728	0.718	0.731	0.719

Table 2. The wavenumber and the reflection rate of the peak Bragg resonance.

explore the influencing factors on the magnitude of the downshift of the wave frequency based on the present solutions.

3.3. *Frequency downshift of the Bragg resonance*

3.3.1. *Derivation of the downshift magnitude*

In this section, we first present a theoretical expression of the downshift magnitude of the wave frequency. The solution of reflection rate, denoted as $\tilde{R} = \tilde{R}(\omega')$, is expressed in (3.5). The wave frequency shift at maximum reflection, denoted as δ, can be obtained from the derivative of the reflection rate with respect to ω' being equal to zero,

$$\frac{\mathrm{d}}{\mathrm{d}\omega'}\left[\tilde{R}\left(\omega'\right)\right]^2\bigg|_{\omega'=\delta} = 0. \tag{3.10}$$

Employing the Taylor expansion of ω' and D to approximate the solution,

$$\delta \approx \delta_0 + \delta_2$$

$$= \frac{3\mathrm{i}C_g^+\left(E_3 + \mathrm{i}E_1 C_g^+\right)}{6E_2 E_3 C_g^+ - \mathrm{i}L^2 D_0^+} + \frac{\eth_4 L^4 + \eth_2 L^2}{5C_g^+\left(6E_2 E_3 C_g^+ - \mathrm{i}L^2 D_0^+\right)^2}, \tag{3.11}$$

in which

$$\eth_4 = E_3 D_0^{+3} + \mathrm{i}C_g^+ D_0^{+2}\left(5D_3^+ + 6E_1 D_0^+\right), \tag{3.12}$$

Case	Variables	The Present solution	$D_1^+ = 0$	$D_2^+ = 0$	$D_3^+ = 0$	$B_1^+ = 0$	$B_2^+ = 0$	$B_3^+ = 0$
D1	$2k^+/k_d$	0.983	0.991	0.987	0.990	0.983	0.981	0.984
L1	$\omega^+/2\pi$	1.151	1.162	1.157	1.156	1.151	1.150	1.150

Table 3. The influence of B_s^+ and D_s^+ on the wavenumber or the wave frequency of the Bragg resonance.

and

$$\eth_2 = 15 \left\{ -E_3^3 D_0^+ - 2iE_1 E_3^2 C_g^+ D_0^+ + iE_1 C_g^{+3} D_3^+ \left(E_1 + 2E_2 D_0^+ \right) \right.$$
$$\left. + E_1 E_3 C_g^{+2} \left[D_3^+ + D_0^+ \left(E_1 - 2E_2 D_0^+ \right) \right] \right\}. \tag{3.13}$$

This is detailed in Appendix C. In Mei's (1985) theory, the coefficients E_1, E_2, E_3 and $D_3^{\pm}$ are equal to 0, and therefore $\eth_4 = \eth_2 = 0$, causing $\delta = 0$.

3.3.2. *Formation of the downshift behaviour*

As has been demonstrated, the additional terms, i.e. $B_s^{\pm}$ and $D_s^{\pm}$ ($s = 1, 2, 3$) in the present solutions are proven to be the causes of downshift behaviour. The following work is to identify the most influential term with respect to the wavenumber or wave frequency in the cases of D1 and L1 by setting each term to zero one by one, of which the terms related to the superscript + are considered.

Table 3 presents the impact of B_s^+ and D_s^+ ($s = 1, 2, 3$) on the wavenumber or wave frequency of the Bragg resonance. The downshift behaviour is impacted by each of the terms, with D_1^+ holding primacy over the two cases. The bottom-induced terms, D_s^+, are more influential than the dispersion-related items, B_s^+. To further explore the significance of these terms, their generation process in the present equations is investigated.

Figure 3 demonstrates the correlations among the terms of the equations, operators and wave components. The generation of these elements is induced by three second-order differential operators for potential functions, defined in fluids ($\mathcal{L}_{flu}$), on the surface ($\mathcal{L}_{sur}$) and at the bottom ($\mathcal{L}_{bot}$), as well as first-order operators ($\bar{\mathcal{L}}_{flu}$ and $\bar{\mathcal{L}}_{bot}$), the details of which are provided in Appendix D. Seven wave components in the potential function contribute to B_s^+ and D_s^+, comprising second-order modes, namely, the non-resonant element $\gamma_{3,1}^{2,+} S_{3,1}^+$ and resonant elements $\gamma b^{\pm} S_{1,1}^{\pm}$ and $\gamma f^{\pm} S_{1,1}^{\pm}$, as well as first-order resonant modes, i.e. $\gamma_{1,1}^{1,\pm} S_{1,1}^{\pm}$. The second-order modes are induced by $\gamma_{1,1}^{1,\pm} S_{1,1}^{\pm}$ through first-order operators $\bar{\mathcal{L}}_{flu}$ and $\bar{\mathcal{L}}_{bot}$, and the non-resonant mode $\gamma_{3,1}^{2,+} S_{3,1}^+$ is expressed as

$$\gamma_{3,1}^{2,+} = \frac{3igDk^2 \mathrm{sech}kh \left(3gk \cosh 3kz + \omega^2 \sinh 3kz \right)}{4\omega \left(3k\omega^2 \cosh 3kh - 9gk^2 \sinh 3kh \right)} A^+, \tag{3.14}$$

which is generated by $\gamma_{1,1}^{1,+} S_{1,1}^+ \xrightarrow{\bar{\mathcal{L}}_{bot}} \gamma_{3,1}^{2,+} S_{3,1}^+$. The resonant modes include four components, given by

$$\gamma_{1,1}^{2,\pm} S_{1,1}^+ = \gamma b^{\pm} S_{1,1}^+ + \gamma f^{\pm} S_{1,1}^+, \tag{3.15}$$
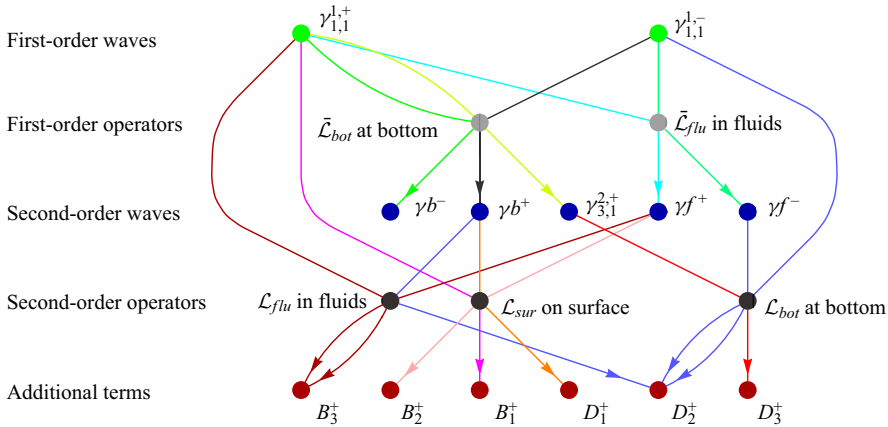
979 A13-15

Figure 3. Illustration of the correlations between the wave components and the additional terms (red points).

in which $\gamma_{1,1}^{2,\pm} S_{1,1}^{\pm}$ is composed of a bottom-forced component $(\gamma b^{\pm} S_{1,1}^{\pm})$ and a fluid-modulated component $(\gamma f^{\pm} S_{1,1}^{\pm})$,

$$\gamma b^{\pm} = -\frac{ikDg \sinh k(z+h)}{4\omega \cosh kh} A^{\mp}, \tag{3.16}$$

and

$$\gamma f^{\pm} = \mp \frac{g(z+h) \sinh k(z+h)}{2\omega \cosh kh} \frac{\partial A^{\pm}}{\partial \xi_1}, \tag{3.17}$$

which are induced via $\gamma_{1,1}^{1,\pm} S_{1,1}^{\pm} \xrightarrow{\bar{\mathcal{L}}_{flu}} \gamma f^{\pm} S_{1,1}^{\pm}$ and $\gamma_{1,1}^{1,\mp} S_{1,1}^{\mp} \xrightarrow{\bar{\mathcal{L}}_{bot}} \gamma b^{\pm} S_{1,1}^{\pm}$, respectively. The generations of B_1^{+}, B_2^{+} and B_3^{+} are described as

$$\gamma_{1,1}^{1,+} S_{1,1}^{+} \xrightarrow{\mathcal{L}_{sur}} B_1^{+}, \quad \gamma f^{+} S_{1,1}^{+} \xrightarrow{\mathcal{L}_{sur}} B_2^{+}, \quad \left(\gamma_{1,1}^{1,+} S_{1,1}^{+}, \gamma f^{+} S_{1,1}^{+}\right) \xrightarrow{\mathcal{L}_{flu}} B_3^{+}. \tag{3.18a–c}$$

The generation of D_1^{+} is demonstrated by $\gamma_{1,1}^{1,-} S_{1,1}^{-} \xrightarrow{\bar{\mathcal{L}}_{bot}} \gamma b^{+} S_{1,1}^{+} \xrightarrow{\mathcal{L}_{sur}} D_1^{+}$. This process is initiated by the first-order reflected wave, $\gamma_{1,1}^{1,-} S_{1,1}^{-}$, which is further reflected by the positive component of the bottom, e^{2ikx}, resulting in the forward mode $\gamma b^{+} S_{1,1}^{+}$. Finally, the wave is temporally modulated at the surface boundary to generate the term, D_1^{+}. The detailed generation process of D_1^{+} revealed the impact mechanisms of D_1^{+} on downshifting behaviour, that is the combination of the bottom re-reflection effect and the surface modulation effect.

The generation of D_2^{+} is more intricate and involves three distinct paths: $\gamma_{1,1}^{1,-} S_{1,1}^{-} \xrightarrow{\mathcal{L}_{bot}}$ D_2^{+}, $\gamma_{1,1}^{1,-} S_{1,1}^{-} \xrightarrow{\bar{\mathcal{L}}_{bot}} \gamma b^{+} S_{1,1}^{+} \xrightarrow{\mathcal{L}_{flu}} D_2^{+}$ and $\gamma_{1,1}^{1,-} S_{1,1}^{-} \xrightarrow{\bar{\mathcal{L}}_{flu}} \gamma f^{-} S_{1,1}^{-} \xrightarrow{\mathcal{L}_{bot}} D_2^{+}$, which is a combination of the first- and second-order contributions from the fluid and bottom.

D_3^{+} is generated by $\gamma_{1,1}^{1,+} S_{1,1}^{+}$, with paths $\gamma_{1,1}^{1,+} S_{1,1}^{+} \xrightarrow{\bar{\mathcal{L}}_{bot}} \gamma_{3,1}^{2,+} S_{3,1}^{+} \xrightarrow{\mathcal{L}_{bot}} D_3^{+}$, indicating that the first-order incident wave is induced by the first-order bottom effect to generate the non-resonant forward wave, $\gamma_{3,1}^{2,+} S_{3,1}^{+}$. This wave is further forced by the second-order bottom effect to strengthen the resonant modes.
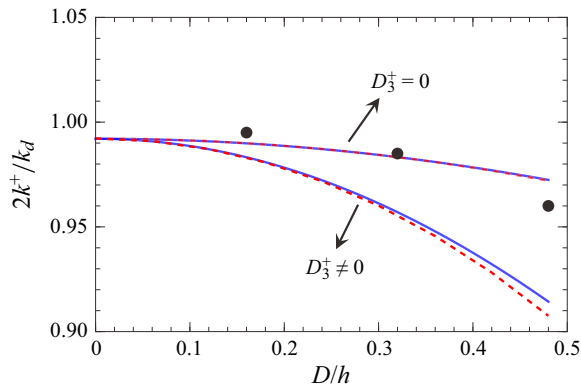
979 A13-16

Figure 4. Comparison of wavenumber of the incident wave of the Bragg resonance among the analytical solution of (3.11) (blue solid line), the numerical results of (3.10) (red dashed line) that includes the influence of the non-resonant mode ($D_3^+ \neq 0$) or excludes this mode ($D_3^+ = 0$), and results of Liu *et al.* (2019) from the MMSE (black dots).

To examine the effect of D_3^+ on the frequency downshift, we compare our results with the solutions of Liu *et al.* (2019), in which the modified mild-slope equation (MMSE) was applied to investigate the effect of bottom height on the downshift behaviour of the Bragg resonance. The experimental settings of case-D1 are adopted, with $h = 0.312$ m, $L = 10$ m, $\lambda_d = 1$ m and $N_d = 10$ fixed, with varying sandbar amplitude D.

As shown in figure 4, with the increase of sandbar amplitude, significant divergence between the present solution and the results of Liu *et al.* (2019) is observed, which is probably attributed to the influence of the non-resonant wave mode, $\gamma_{3,1}^{2,+} S_{3,1}^+$, which was not included in the MMSE. By setting D_3^+ to zero to eliminate the effect of this non-resonant wave, the present analytical and numerical results show satisfactory agreement with the solutions obtained by the MMSE. This reveals that the non-resonant mode is a dominant factor responsible for the downward shift in the wavenumber of the Bragg resonance for steep sandbar amplitude.

3.3.3. *Impact of the sandbar amplitude on the magnitude of the Bragg resonance downshift*

The approximate expression for the magnitude of the wave frequency downshift (3.11), which is of a parabolic form, i.e. $\delta \approx \delta_0 + \delta_2$, with $\delta_0 = O(1)$ and $\delta_2 = O(D^2)$, reveals that with the increase of sandbar amplitude D, the parabolic or squared trend of δ is more pronounced than its linear trend since δ_1 (the primary term of D) is always equal to zero. In addition, a threshold downshift magnitude is observed; for $D \to 0$, δ converges to δ_0, which is negative for finite sandbar lengths ($L < \infty$), indicating that for finite sandbar lengths, any amplitude can result in a downward shift, while for $L \to \infty$, where δ_0 tends to 0, and the downshift threshold is eliminated.

To further examine the theoretical expression of the downshift magnitude and provide further insight into the phenomenon, the solutions of reflection rate and resonance frequency for gradually increased D/h are presented. In case L1, the parameters $h, L, \lambda_d, N_d, k_d$, and k are set to 0.22 m, 2.5 m, 0.5 m, 10, 4π m^{-1}, and 2π m^{-1}. The reflection rate for various sandbar amplitudes D is then calculated for a range of wave frequencies.
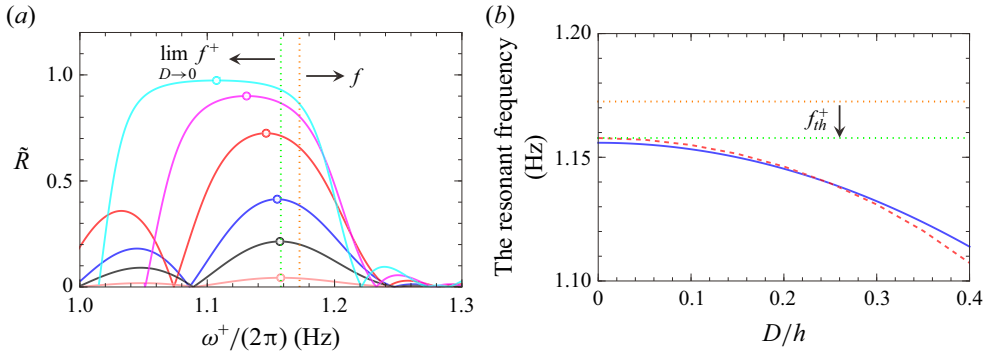
Figure 5. (*a*) Reflection coefficient (3.5) vs wave frequency for various D/h values, with circles denoting the peak value, and the solid lines, from top to bottom, represent $D/h = 0.4, 0.3, 0.2, 0.1, 0.05, 0.01$. (*b*) Comparison of the analytical solution in (3.11) (blue solid line) and numerical results from (3.10) (red dashed line) on the frequency of the Bragg resonance vs sandbar amplitude. Green and orange dotted lines represent the threshold frequency and wave frequency, respectively.

Figure 5(*a*) presents the variation of the reflection coefficients with respect to the ratio of the sandbar amplitude D to the water depth h. The shift of the open markers indicates an enhancement of downshift behaviour of the Bragg resonance with the increase of D/h. Conversely, with the decrease of D/h, the frequency of the reflection peaks increases up to a limit of 1.1578 Hz, as shown in figure 5(*b*) (depicted by the green dotted line), with f_{th}^+ denoting the downward shift of the wave frequency to the threshold frequency. This frequency can be obtained both analytically (blue solid line from the theoretical expression (3.11)) and numerically (red dashed line, by conducting the numerical procedure for (3.10)). Overall agreement between the two solutions is observed, confirming the parabolic trend of the Bragg resonance frequency as a function of the sandbar amplitude. In addition, the wave frequency $f = \omega/2\pi = 1.1725$ Hz, which is the frequency without downshift and depicted by the orange dotted line in both figure 5(*a*,*b*), is always above the other curves, indicating the downshift behaviour for any sandbar amplitude D. The agreement between the two solutions in figure 5(*b*) further demonstrates the hypothesis of the existence of a threshold frequency.

4. Analyses of the fully nonlinear ENLS equations

In the previous work, we neglected the influence of nonlinearity on Bragg resonance for the convenience of analytical solution. However, wave nonlinearity is a key factor that affects wave transformation and reflection by altering wave speed and can cause nonlinear behaviours. In this section, the influence of nonlinearity on Bragg resonance is analysed and discussed. First, based on the Bragg resonance criteria and the nonlinear dispersion relation derived from the full nonlinear ENLS equation, we present a theoretical analysis on nonlinear Bragg scattering by the sandbars with infinitesimal amplitude. Then, the full nonlinear ENLS equation is solved numerically to investigate the wave nonlinearity impact on wave reflection by sandbars with finite amplitude.

Let $R_{re}(x)$, $T_{re}(x)$ and $R_{im}(x)$, $T_{im}(x)$ denote the real and imaginary parts of $R(x)$ and $T(x)$, respectively. $A^\pm$ can be expressed as

$$A^+ = A_0 \left[T_{re}(x) + iT_{im}(x) \right] e^{-i\omega' t}, \quad (0 < x < L) \tag{4.1}$$

979 A13-18

and

$$A^- = A_0 \left[R_{re}(x) + iR_{im}(x) \right] e^{-i\omega' t}. \quad (0 < x < L). \tag{4.2}$$

Substituting (4.1) and (4.2) into (2.42) and (2.43), and separating real and imaginary items, we can obtain a set of nonlinear differential equations. The reflection coefficient can be obtained by:

$$\tilde{R} = \left| R_{re}(0) + iR_{im}(0) \right|. \tag{4.3}$$

4.1. *Theoretical analysis on the critical kh of resonance shift under infinitesimal sandbar amplitude condition*

In this section, to examine the impact of wave nonlinearity on resonant wavenumber shift, the Bragg resonance criterion proposed by Mei (1985) is applied to consider a limiting condition: large number of sandbars with infinitesimal amplitude ($k_d D \to 0$).

According to the analysis in §3, under this condition, the following criterion, which indicates the wavenumber of the maximum reflection, can precisely predict the wavenumber of the incident wave:

$$k^+ + k^- = k_d. \tag{4.4}$$

On the side where $x < 0$, waves propagate over constant water depth, and the dispersion relation for nonlinear waves can be obtained, where the wavenumbers of the incident and reflected waves can be expressed as

$$\left.\begin{aligned}
k^+ &= k + \frac{iE_2 \left(\omega'\right)^2 + \omega'}{C_g^+} + A_0^2 \overbrace{\left(\frac{iF_1^+}{C_g^+} + \frac{iF_2^+}{C_g^+} \tilde{R}^2 \right)}^{\text{wave nonlinearity induced}}, \\
k^- &= k + \frac{iE_2 \left(\omega'\right)^2 + \omega'}{C_g^+} + A_0^2 \underbrace{\left(\frac{iF_1^+}{C_g^+} \tilde{R}^2 + \frac{iF_2^+}{C_g^+} \right)}_{},
\end{aligned}\right\} \tag{4.5}$$

where the third terms on the right-hand sides are the additional wavenumbers induced by the nonlinearity of incident and reflected waves, usually we have $k^+ \neq k^-$. This is a typical characteristic different from small amplitude waves condition, where the wavenumbers are identical. However, when waves approach a full reflection condition, with $\tilde{R} \to 1$, the difference induced by wave nonlinearity tends to 0, namely $k^+ - k^- \to 0$.

Combining the Bragg resonance criterion (4.4) and the dispersion relation (4.5), the non-dimensional incident wavenumber $2k^+/k_d$ under resonant condition can be obtained:

$$\frac{2k^+}{k_d} = 1 + \frac{k^+ - k^-}{k_d} = 1 + \frac{1 - \tilde{R}^2}{C_g^+ k_d} \left(iF_1^+ - iF_2^+ \right) A_0^2, \tag{4.6}$$

where iF_1^+ and iF_2^+ are the self- and cross-modulation coefficients (Hammack *et al.* 2005; Onorato *et al.* 2006). As can be seen, for small amplitude waves ($A_0 \to 0$), the resonance occurs at $2k^+/k_d = 1$, as the incident wavenumber is identical to that of reflected waves. While for waves with finite wave amplitude ($A_0 = O(1)$), wave self- and cross-modulation effects induce an additional shift of the resonant wavenumber, for which the shift direction is determined by $iF_1^+ - iF_2^+$, whereas the former effect dominates wavenumber upshifting and the latter downshifting.
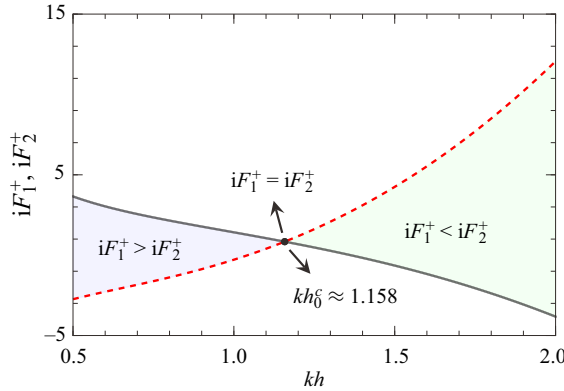
Figure 6. The self-modulation $\mathrm{i}F_1^+$ (black line) and cross-modulation coefficients $\mathrm{i}F_2^+$ (red dashed line) vary with kh.

As illustrated in figure 6, the values of $\mathrm{i}F_1^+$ and $\mathrm{i}F_2^+$ vary with kh. Let $\mathrm{i}F_1^+ = \mathrm{i}F_2^+$, combined with their definitions in (2.39), the solution for critical kh, which represents the condition of the prefect balance of self-modulation and cross-modulation, of resonance shift under infinitesimal sandbar amplitude condition can be obtained theoretically:

$$kh_0^c = 1.15798\cdots \approx 1.158. \tag{4.7}$$

Combining the relationship presented in figure 6 and (4.6), we can find that opposing shift behaviours will occur on the two sides of $kh = kh_0^c$, owing to the discrepancy between the incident and reflected wavenumbers induced by the differences between wave self- and cross-modulation effects. More specifically, when $kh < kh_0^c$, the self-modulation effect is stronger than wave cross-modulation, resulting in $k^+ > k^-$, therefore, $2k^+/k_d$ shifts upward with the increase of wave amplitude A_0. While when $kh > kh_0^c$, the cross-modulation effect becomes more pre-dominant and results in $k^+ < k^-$, therefore, $2k^+/k_d$ shows downshift behaviour with the increase of A_0, where we have $k^+ < k^-$.

4.2. *Numerical study on critical kh of resonance shift under finite sandbar amplitude condition*

Under infinitesimal sandbar amplitude condition ($k_d D \to 0$), the existence of the critical kh has been theoretically demonstrated. To further consider the condition of sandbars with finite amplitude ($k_d D = O(1)$), numerical approach is needed to solve the fully nonlinear ENLS for reflection coefficient, and the details of the numerical procedure is outlined in Appendix E.

Following the set-up of experimental case D1, we set $k_d = 2\pi\,\mathrm{m}^{-1}$ and $k = \pi\,\mathrm{m}^{-1}$, and the number of sandbars is fixed at 25. Seven cases with different sandbar amplitude D were adopted, to calculate the reflection coefficients under the conditions with varying water depth, i.e. $kh = 0.8 \sim 2.2$, for incident waves with different wavenumber ($2k^+/k_d = 0.9 \sim 1.1$) and different wave amplitude ($kA_0 = 0 \sim 0.08$). The parameters of our numerical solutions are detailed in table 4, in which the calculated critical kh are listed in the last columns.

Figure 7 shows the reflection coefficients for three different cases, namely kh is lower than, equal to and higher than the critical value kh^c, to illustrate the numerical procure of calculating the critical kh. First, we calculate the reflection coefficient under a small

979 A13-20

Case	k_dD	kA_0	$2k^+/k_d$	kh	kh^c
(I)	10^{-6}	$0 \sim 0.08$	$0.9 \sim 1.1$	$0.8 \sim 2.2$	1.158
(II)	0.04	$0 \sim 0.08$	$0.9 \sim 1.1$	$0.8 \sim 2.2$	1.168
(III)	0.08	$0 \sim 0.08$	$0.9 \sim 1.1$	$0.8 \sim 2.2$	1.196
(IV)	0.12	$0 \sim 0.08$	$0.9 \sim 1.1$	$0.8 \sim 2.2$	1.243
(V)	0.16	$0 \sim 0.08$	$0.9 \sim 1.1$	$0.8 \sim 2.2$	1.305
(VI)	0.20	$0 \sim 0.08$	$0.9 \sim 1.1$	$0.8 \sim 2.2$	1.373
(VII)	0.24	$0 \sim 0.08$	$0.9 \sim 1.1$	$0.8 \sim 2.2$	1.444

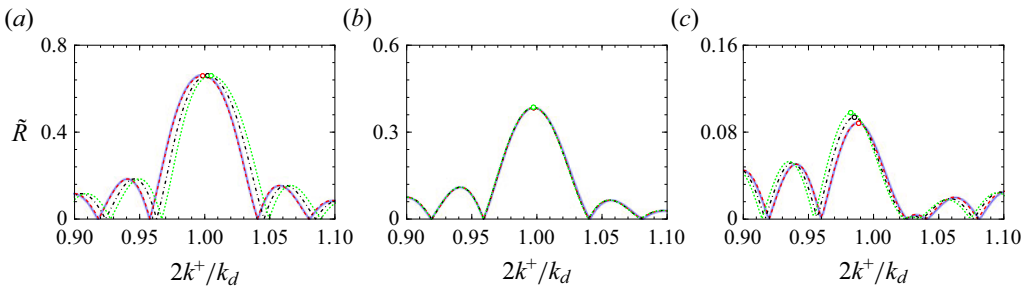Table 4. Incident wave and bottom conditions.

Figure 7. Comparisons of reflection coefficients vs incident wavenumber for case (III) with different kh among linear analytical solution in (3.5) (blue solid line), numerical solutions for $kA_0 = 0$ (red dashed line), 0.06 (black dot-dashed line) and 0.08 (green dotted line): (*a*) $kh = 0.8$; (*b*) $kh = 1.196$; (*c*) $kh = 2.2$.

kh condition, i.e. $kh = 0.8$ for waves with different wavenumber and wave amplitude. Figure 7(*a*) shows that as the wave steepness increases, the wavenumber of the Bragg resonance shifts upward, in which intensifying the wave steepness significantly increases the wavenumber of the Bragg resonance. Second, the results with a large kh are calculated. As shown in figure 7(*c*), the wavenumber of the Bragg resonance decreases monotonically with increasing wave steepness, showing a downward shift. Then, we consider the condition of a medium kh, i.e. $kh = (0.8 + 2.2)/2 = 1.5$, if downshift occurs then the critical kh is located between 0.8 and 1.5, otherwise we consider the region of [1.5, 2.2]. We repeat the above procedure until we find an approximate value of kh^c. Specifically, for case (III), $kh = kh^c \approx 1.196$, as shown in figure 7(*b*), where the increase of wave nonlinearity will not induce a shift to the resonant wavenumber.

Thus, for sandbars with finite amplitude, the critical kh, kh^c still exists, which corresponds to the condition where wave nonlinearity will not induce a shift to the resonant wavenumber. Following the same calculation procedure, the relationship between kh^c and k_dD is obtained for cases (I)–(VII) regarding reflection coefficients for kh ranging from 0.8 to 2.2, as illustrated in figure 8, with the critical kh being the dividing line of upshift and downshift behaviour.

As illustrated in figure 8, the critical kh, kh^c shows an overall increase trend with the increase of sandbar amplitude. Under the condition of mild sandbar amplitude, i.e. $k_dD < 0.04$, the critical kh presents slight variation, and kh^c tends to the critical kh, $kh_0^c \approx 1.158$, which has also been predicted by theoretical analysis with (4.7) as $k_dD \to 0$. For $kh < kh^c$, the frequency of Bragg resonance presents an upshift with the increase of wave nonlinearity. Whereas for kh larger than kh^c, the regime of frequency shift induced by wave nonlinearity transits to a downshift one.
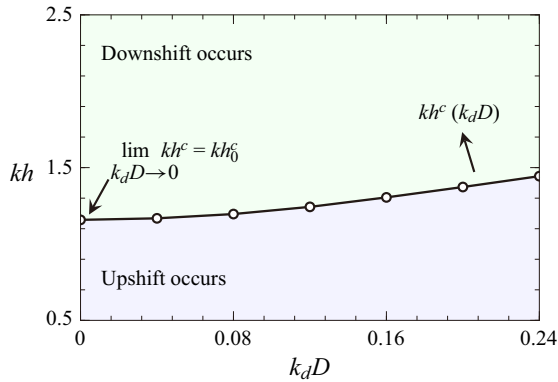
Figure 8. Critical $kh(kh^c)$ varies with k_dD.

5. Conclusion

In this work, the ENLS equations have been derived by employing the multiple-scale expansion method to describe wave scattering by sinusoidal sandbars. A closed-form solution has been established by solving the linearised ENLS equations and a theoretical formula for the downshift magnitude of the resonance frequency has been proposed. The factors that influence the downshift of the Bragg resonance have been examined and the underlying mechanisms are revealed. Finally, fully nonlinear ENLS equations are solved numerically to investigate the effect of wave nonlinearity on wave reflection. The main conclusions are drawn as follows.

(i) Among the effects of high-order bottom, high-order dispersion and nonlinear wave–wave interaction on Bragg scattering, the high-order bottom effect is the major cause of the downshift behaviour, attributed to the combination of the re-reflection of waves and the surface modulation effect. In addition, the interaction between the forward non-resonant mode and sinusoidal sandbars also plays an important role in causing downshift behaviour, especially when the sandbar amplitude varies steeply, where a significant increase in the downward shift appears that leads to an underestimation of the downshift behaviour by the MMSE.

(ii) An analytical formula for the wave frequency downshift has been presented that exhibits a parabolic form with respect to the amplitude and length of sandbars, which remains valid even if the bar length approaches infinity. As the bar amplitude tends to zero, the magnitude of the frequency downshift converges to a negative threshold. This phenomenon is caused by the finite length of the sandbars and vanishes as the length approaches infinity. In addition, an expression for the wavenumber of the reflection peaks has been derived via the dispersion relation, which degenerates to the standard Bragg law as the sandbar length approaches infinity and the bar amplitude approaches zero, validating the standard Bragg law under this condition.

(iii) The nonlinearity of the waves has been observed to cause a shift of the Bragg resonance, with both an upward and a downward behaviour, attributed to the discrepancy between the wavenumbers of the incident and reflected waves, which is highly represented by kh. Under an infinitesimal sandbar amplitude condition, theoretical analysis has revealed the existence of a critical kh, kh_0^c, which corresponds to the condition where self-modulation equals the cross-modulation effect, where on the two sides, wave nonlinearity presents converse behaviours

regarding wavenumber shift of the Bragg resonance. The self-modulation effect is responsible for wavenumber upshifting and the cross-modulation effect dominates downshifting. When kh is above kh^c, the increase of wave nonlinearity causes a significant downshift of the Bragg resonance, where it is dominated by the cross-modulation effect with the reflected wavenumber larger than that of the incident wave. With the decreases of kh, the waves gradually transition from being cross-modulated-dominated to self-modulated-dominated; as a result, the incident wavenumber gradually increases and becomes larger than the reflected wavenumber, together with the gradual change of Bragg resonance frequency from downshift to upshift. Therefore, when kh is smaller than the critical kh, the enhancement of wave nonlinearity triggers an upshift behaviour. Furthermore, numerical results have proved the relation between the critical kh and sandbar amplitude D, which will move upwards with an increase of the amplitude of sandbars.

Declaration of interests. The authors report no conflict of interest.

Author ORCIDs.
Haiqi Fang https://orcid.org/0009-0005-7182-5004;
Lian Tang https://orcid.org/0009-0001-1366-889X.

Author contributions. Haiqi Fang: methodology, validation, formal analysis, writing – original draft, manuscript preparation. Lian Tang: formal analysis, writing – review and editing, specifically critical review, commentary or revision. Pengzhi Lin: conceptualisation, supervision. All authors reviewed the results and approved the final version of the manuscript.

Appendix A. Solution procedure for the *j*th-order problem for ϕ_j

In general, we consider the *j*th-order problem for ϕ_j, defined by the following equations,

$$\frac{\partial^2 \phi_j}{\partial x^2} + \frac{\partial^2 \phi_j}{\partial z^2} = T_j \quad (-h < z < 0), \tag{A1}$$

$$\frac{\partial^2 \phi_j}{\partial t^2} + g\frac{\partial \phi_j}{\partial z} = P_j \quad (z = 0), \tag{A2}$$

$$\frac{\partial \phi_j}{\partial z} = W_j \quad (z = -h). \tag{A3}$$

Here ϕ_j is assumed to be expressed as series form in terms of multiple harmonics,

$$\phi_j = \gamma_{0,0}^{j,+} + \sum_{\substack{mn=0 \\ m+n>0}} \left(\gamma_{m,n}^{j,+} S_{m,n}^+ + \text{c.c.}\right) + \sum_{m=1}^{\infty}\sum_{n=1}^{\infty} \left(\gamma_{m,n}^{j,+} S_{m,n}^+ + \gamma_{m,n}^{j,-} S_{m,n}^- + \text{c.c.}\right), \tag{A4}$$

where $\gamma_{m,n}^{j,\pm} = \gamma_{m,n}^{j,\pm}(z, \xi_1, \tau_1, \xi_2, \tau_2)$ are functions corresponding to $S_{m,n}^{\pm}$ for the *j*th-order problem. Substituting (A4) into (A1)–(A3) and separating different orders of harmonics,

$S_{m,n}^{\pm}$, a set of ordinary differential equations for $\gamma_{m,n}^{j,\pm}$ can be obtained:

$$\left(\frac{\partial^2}{\partial z^2} - m^2 k^2\right) \gamma_{m,n}^{j,\pm} = T_{m,n}^{j,\pm} \quad (-h < z < 0), \tag{A5}$$

$$g\frac{\partial \gamma_{m,n}^{j,\pm}}{\partial z} - n^2 \omega^2 \gamma_{m,n}^{j,\pm} = P_{m,n}^{j,\pm} \quad (z = 0), \tag{A6}$$

$$\frac{\partial \gamma_{m,n}^{j,\pm}}{\partial z} = W_{m,n}^{j,\pm} \quad (z = -h). \tag{A7}$$

The method of solving (A5)–(A7) is highly dependent on the values of the parameters m and n. For the jth-order problem, the solutions of $T_{m,n}^{j,\pm}$, etc., differ depending on whether mn is equal to 1 or not. In the case that $mn \neq 1$, the solutions of $\gamma_{m,n}^{j,\pm}$ are non-singular, obtained directly by solving the BVP. Conversely, when $mn = 1$, the equations become singular, thereby requiring two additional solvability conditions to be satisfied to guarantee the existence of the solution of $\gamma_{m,n}^{j,\pm}$.

A.1. *For* $mn \neq 1$

When $mn \neq 1$, the non-homogeneous equation with non-zero boundary conditions can be linearly decomposed into two distinct problems. The first is a homogeneous equation, with two non-zero boundary conditions, and the other a non-homogeneous equation with two zero boundary conditions. Representing each problem is $\gamma_{m,n}^{j,\pm}$, with $\bar{\gamma}_{m,n}^{j,\pm}$ being the solution for the homogeneous equation and $\bar{\bar{\gamma}}_{m,n}^{j,\pm}$ for the non-homogeneous equation:

$$\gamma_{m,n}^{j,\pm} = \bar{\gamma}_{m,n}^{j,\pm} + \bar{\bar{\gamma}}_{m,n}^{j,\pm}. \tag{A8}$$

For $\bar{\gamma}_{m,n}^{j,\pm}$, we have

$$\left(\frac{\partial^2}{\partial z^2} - m^2 k^2\right) \bar{\gamma}_{m,n}^{j,\pm} = 0 \quad (-h < z < 0), \tag{A9}$$

$$g\frac{\partial \bar{\gamma}_{m,n}^{j,\pm}}{\partial z} - n^2 \omega^2 \bar{\gamma}_{m,n}^{j,\pm} = P_{m,n}^{j,\pm} \quad (z = 0), \tag{A10}$$

$$\frac{\partial \bar{\gamma}_{m,n}^{j,\pm}}{\partial z} = W_{m,n}^{j,\pm} \quad (z = -h). \tag{A11}$$

The general solution of (A9) is $\bar{\gamma}_{m,n}^{j,\pm} = \bar{C}_1 \cosh mk(z+h) + \bar{C}_2 \sinh mk(z+h)$, and $\bar{C}_1$ and $\bar{C}_2$ are two arbitrary complexes, determined by two boundaries, which can be uniquely ensured after substituting the general solution of $\bar{\gamma}_{m,n}^{j,\pm}$ to (A10) and (A11). The simplified solution for $\bar{\gamma}_{m,n}^{j,\pm}$ is derived,

$$\bar{\gamma}_{m,n}^{j,\pm} = \frac{P_{m,n}^{j,\pm}}{gmk\tanh mkh - n^2\omega^2} \frac{\cosh mk(z+h)}{\cosh mkh}$$

$$+ W_{m,n}^{j,\pm}\left\{\frac{\sinh mk(z+h)}{mk} + \frac{n^2\omega^2 \tanh mkh - gmk}{gm^2 k^2 \tanh mkh - mkn^2\omega^2}\cosh mk(z+h)\right\}. \tag{A12}$$

The second problem is expressed as follows:

$$\left(\frac{\partial^2}{\partial z^2} - m^2 k^2\right) \bar{\bar{\gamma}}_{m,n}^{j,\pm} = T_{m,n}^{j,\pm} \quad (-h < z < 0), \tag{A13}$$

$$g \frac{\partial \bar{\bar{\gamma}}_{m,n}^{j,\pm}}{\partial z} - n^2 \omega^2 \bar{\bar{\gamma}}_{m,n}^{j,\pm} = 0 \quad (z = 0), \tag{A14}$$

$$\frac{\partial \bar{\bar{\gamma}}_{m,n}^{j,\pm}}{\partial z} = 0 \quad (z = -h). \tag{A15}$$

In this paper, we consider $T_{m,n}^{j,\pm}$ of hyperbolic cosine function form, namely $\mu \cosh k(z + h)$, where μ is a constant. The general solution of (A13) is

$$\bar{\bar{\gamma}}_{m,n}^{j,\pm} = \left(\bar{\bar{C}}_1 + \frac{\mu z}{2km}\right) \sinh mk(z + h) + \left(\bar{\bar{C}}_2 - \frac{\mu}{4k^2 m^2}\right) \cosh mk(z + h), \tag{A16}$$

in which $\bar{\bar{C}}_1$ and $\bar{\bar{C}}_2$ are coefficients, which can be determined by boundaries (A14) and (A15).

Substituting (A16) into (A15), $\bar{\bar{C}}_1$ can be obtained

$$\bar{\bar{C}}_1 = \frac{\mu h}{2km}. \tag{A17}$$

By substituting the solution of $\bar{\bar{C}}_1$, (A17), into (A16), and applying the surface boundary condition (A14), the value of $\bar{\bar{C}}_2$ can be decided as

$$\bar{\bar{C}}_2 = -\frac{\mu}{4k^2 m^2} \frac{km\left(g - 2hn^2\omega^2\right) \tanh mkh + 2ghk^2 m^2 + n^2\omega^2}{gkm \tanh mkh - n^2\omega^2}. \tag{A18}$$

Therefore, all the coefficients are obtained, which leads to the unique solution from (A16)–(A18). The unique solution of $\bar{\bar{\gamma}}_{m,n}^{j,\pm}$ can be obtained,

$$\bar{\bar{\gamma}}_{m,n}^{j,\pm} = \frac{\mu(z+h)}{2km} \sinh mk(z+h) - \frac{\mu}{2km} \frac{gkmh + \left(g - n^2\omega^2 h\right) \tanh kmh}{gkm \tanh mkh - n^2\omega^2} \cosh mk(z+h). \tag{A19}$$

It is worth noting that the solution in (A19) is valid as $mn \neq 1$, since the denominator of the second term on the right-hand side is not equal to zero.

Thus, the BVP for the harmonics $S_{m,n}^{\pm}$ at jth order is solved, giving the solution for $\gamma_{m,n}^{j,\pm}$ in the case of $mn \neq 1$.

$$\bar{\gamma}_{m,n}^{j,\pm} = \frac{P_{m,n}^{j,\pm}}{gmk \tanh mkh - n^2\omega^2} \cosh mk(z+h)$$

$$- W_{m,n}^{j,\pm} \left\{ \frac{\sinh mk(z+h)}{mk} + \frac{n^2\omega^2 \tanh mkh - gmk}{gm^2 k^2 \tanh mkh - mkn^2\omega^2} \cosh mk(z+h) \right\}$$

$$+ \frac{\mu(z+h)}{2km} \sinh mk(z+h) - \frac{\mu}{2km} \frac{gkmh + \left(g - n^2\omega^2 h\right) \tanh kmh}{gkm \tanh mkh - n^2\omega^2} \cosh mk(z+h). \tag{A20}$$

A.2. *For mn = 1*

For the case of $mn = 1$ or $m = n = 1$, the solution for $\gamma_{1,1}^{j,\pm}$ displayed in (A20) is subjected to divergence due to the dispersion relation. The governing equation and boundary are as follows:

$$\left(\frac{\partial^2}{\partial z^2} - k^2\right)\gamma_{1,1}^{j,\pm} = T_{1,1}^{j,\pm} \quad (-h < z < 0), \tag{A21}$$

$$g\frac{\partial \gamma_{1,1}^{j,\pm}}{\partial z} - \omega^2 \gamma_{1,1}^{j,\pm} = P_{1,1}^{j,\pm} \quad (z = 0), \tag{A22}$$

$$\frac{\partial \gamma_{1,1}^{j,\pm}}{\partial z} = W_{1,1}^{j,\pm} \quad (z = -h). \tag{A23}$$

Let $\psi^\pm$ represent the homogenous solutions of (A21)–(A23). Multiplying (A21) by $\psi^\pm$ and integrating it between $-h$ and 0, the Green formula can be applied in accordance with the divisional integral formula, leading to the solvability of the BVP at $O(\varepsilon^j)$ for $\gamma_{1,1}^{j,\pm}$

$$\int_{-h}^{0} \left\{ \left(\frac{\partial^2 \gamma_{1,1}^{j,\pm}}{\partial z^2} - k^2\gamma_{1,1}^{j,\pm}\right)\psi^\pm - \left(\frac{\partial^2 \psi^\pm}{\partial z^2} - k^2\psi^\pm\right)\gamma_{1,1}^{j,\pm} \right\} \, \mathrm{d}z = \left(\psi^\pm \frac{\partial \gamma_{1,1}^{j,\pm}}{\partial z} - \gamma_{1,1}^{j,\pm}\frac{\partial \psi^\pm}{\partial z}\right)\Bigg|_{-h}^{0}. \tag{A24}$$

Then the simplified solvability condition is expressed as

$$\int_{-h}^{0} T_{1,1}^{j,\pm}\psi^\pm \, \mathrm{d}z = g^{-1}P_{1,1}^{j,\pm}\psi^\pm\Big|_{z=0} - W_{1,1}^{j,\pm}\psi^\pm\Big|_{z=-h}, \tag{A25}$$

if the solvability condition (A25) holds, then the existence of solutions for $\gamma_{1,1}^{j,\pm}$ can be ensured. Thus, the linear differential equation (A5) combined with the Neumann boundary condition at $z = -h$, (A7), is solved for $\gamma_{1,1}^{j,\pm}$.

Similarly, in this paper, the form of $T_{1,1}^{j,\pm}$ is the product of $\cosh k(z + h)$ and a constant μ, namely $T_{1,1}^{j,\pm} = \mu \cosh k(z + h)$, the analytical expression of the general solution for $\gamma_{1,1}^{j,\pm}$ is

$$\gamma_{1,1}^{j,\pm} = C_1 \cosh k(z + h) + \left(\frac{\mu}{2k}(z + h) + \frac{1}{k}W_{1,1}^{j,\pm}\right)\sinh k(z + h), \tag{A26}$$

where the general solution can be indicated by the first term on the right-hand side, where C_1 is an arbitrary complex. The third term arises from the non-zero boundary at $z = -h$. In the case of $mn \neq 1$, the process of solving is analogous to the first problem, as depicted by (A13)–(A18). The distinguishing factor is that the Robin boundary condition (A14) is no longer applicable, thus preventing the determination of the complex C_1. However, the general solution can be included into the ϕ_1 component, which can be disregarded in high-order problems, with $C_1 = 0$ being imposed in order to guarantee a unique solution,

$$\gamma_{1,1}^{j,\pm} = \left[\frac{\mu}{2k}(z + h) + \frac{1}{k}W_{1,1}^{j,\pm}\right]\sinh k(z + h). \tag{A27}$$

Appendix B. Derivation for the solution of the linearised equations

On the left-hand side of the sandbars, we have

$$A^+ = A_0 \exp(\mathrm{i}k'x - \mathrm{i}\omega't) \quad (x < 0), \tag{B1}$$

and

$$A^- = A_0 R(0) \exp(-\mathrm{i}k''x - \mathrm{i}\omega't) \quad (x < 0). \tag{B2}$$

The wavenumbers of the incident and reflected waves are

$$k^\pm = k + \frac{\mathrm{i}E_2\left(\omega'\right)^2 + \omega'}{C_g^+}. \tag{B3}$$

On the side $x > L$, only transmission occurs, indicating that

$$A^+ = A_0 T(L) \exp(\mathrm{i}k'x - \mathrm{i}\omega't) \quad (x > L) \tag{B4}$$

and

$$A^- = 0 \quad (x > L). \tag{B5}$$

Let $\tilde{R}$ and $\tilde{T}$ denote the reflection and transmission rates, given by $|R(0)|$ and $|T(L)|$. The governing equations (3.1) and (3.2) can be expressed in terms of $T(x)$ and $R(x)$. Here $\dot{(\,)}$ represents the first-order differential operator on x, and the equations can be expressed as

$$\left.\begin{aligned} S_1^+ R(x) + S_2^+ T(x) + S_3^+ \dot{R}(x) + S_4^+ \dot{T}(x) = 0, \\ S_1^- T(x) + S_2^- R(x) + S_3^- \dot{T}(x) + S_4^- \dot{R}(x) = 0, \end{aligned}\right\} \tag{B6}$$

where

$$S_1^\pm = E_1\omega' + \mathrm{i}D_0^+, \quad S_2^\pm = -\mathrm{i}\omega' + E_2\left(\omega'\right)^2 + D_3^+, \quad S_3^\pm = \pm E_3, \quad S_4^+ = \pm C_g^+, \tag{B7a–d}$$

in which E_1, E_2 and E_3 are coefficients, defined in (3.7). The boundary conditions for $T(x)$ and $R(x)$ are given by

$$R(L) = 0, \quad T(0) = 1. \tag{B8}$$

The linear equations (B6) with the associated boundary conditions outlined by (B8) constitute a solvable BVP, yielding an exact solution for the reflection rate, $\tilde{R}$.

The linear differential system can be expressed in matrix form,

$$\dot{\mathcal{U}}(x) = \boldsymbol{A}^{-1}\boldsymbol{B}\mathcal{U}(x) \tag{B9}$$

in which $\mathcal{U}(x)$ is a column vector, $\boldsymbol{A}$ and $\boldsymbol{B}$ are matrix, with $\boldsymbol{A}^{-1}$ being the inverse matrix of $\boldsymbol{A}$, given by

$$\left.\begin{aligned} \mathcal{U}(x) = (R(x), T(x))^{\mathrm{T}}, \\ \boldsymbol{A} = \begin{pmatrix} S_3^+ & S_4^+ \\ S_4^- & S_3^- \end{pmatrix}, \quad \boldsymbol{B} = -\begin{pmatrix} S_1^+ & S_2^+ \\ S_2^- & S_1^- \end{pmatrix}. \end{aligned}\right\} \tag{B10}$$

Let us imply a linear transform to $\mathcal{U}(x)$,

$$\mathcal{V}(x) = \boldsymbol{Q}\mathcal{U}(x), \tag{B11}$$

where $\boldsymbol{\mathcal{V}}(x)$ is a column vector with two components $\tilde{R}(x)$ and $\tilde{T}(x)$, and $\boldsymbol{Q}$ is a constant matrix, defined as follows:

$$
\left.
\begin{aligned}
\boldsymbol{\mathcal{V}}(x) &= (\tilde{R}(x),\, \tilde{T}(x))^{\mathrm{T}}, \\
\boldsymbol{Q} &= \begin{pmatrix} -Q_2 + P\,\mathrm{sgn}\left(P^2\right) & -Q_2 - P\,\mathrm{sgn}\left(P^2\right) \\ Q_1 & Q_1 \end{pmatrix}^{-1},
\end{aligned}
\right\}
\tag{B12}
$$

in which Q_1 and Q_2 are real parameters, defined as

$$
Q_1 = \mathrm{i}\frac{S_1^+ S_4^+ + S_2^+ S_3^+}{\left(S_4^+\right)^2 - \left(S_3^+\right)^2},
\tag{B13}
$$

and

$$
Q_2 = \mathrm{i}\frac{S_1^+ S_3^+ + S_2^+ S_4^+}{\left(S_4^+\right)^2 - \left(S_3^+\right)^2}.
\tag{B14}
$$

In addition, P is a complex, given by

$$
P = \sqrt{\frac{\left(S_1^+\right)^2 - \left(S_2^+\right)^2}{\left(S_4^+\right)^2 - \left(S_3^+\right)^2}}.
\tag{B15}
$$

Let us denote the sign function of P^2 as $\mathrm{sgn}(P^2)$, which is equal to 1 for $P^2 > 0$ and to -1 for $P^2 < 0$. Under the linear transform, (B9) is converted into

$$
\dot{\boldsymbol{\mathcal{V}}}(x) = \boldsymbol{C}\boldsymbol{\mathcal{V}}(x),
\tag{B16}
$$

where $\boldsymbol{C} = Q\boldsymbol{A}^{-1}\boldsymbol{B}\,\boldsymbol{Q}^{-1}$, being a diagonal matrix

$$
\boldsymbol{C} = \begin{pmatrix} \mathrm{i}P & 0 \\ 0 & -\mathrm{i}P \end{pmatrix}.
\tag{B17}
$$

Since $(S_4^+)^2 - (S_3^+)^2 > 0$, the sign of $(S_1^+)^2 - (S_2^+)^2$ is the same as P^2, which results in $\mathrm{sgn}((S_1^+)^2 - (S_2^+)^2) = \mathrm{sgn}(P^2)$. Thus, we discuss the solutions in terms of $P^2 > 0$, < 0 and $= 0$, respectively.

The uncoupled linear system is easily solvable with general solution, expressed as

$$
\boldsymbol{\mathcal{V}}(x) = \left(C_1 \mathrm{e}^{\mathrm{i}Px},\, C_2 \mathrm{e}^{-\mathrm{i}Px}\right)^{\mathrm{T}},
\tag{B18}
$$

The general solution of $\boldsymbol{\mathcal{U}}(x)$ can be formulated by utilising the inverse transformation of (B11). This, combined with the conditions specified in (B8), yields the value for C_1

979 A13-28

and C_2. Following this, the solutions for $R(x)$ and $T(x)$ can be obtained:

$$\left.\begin{aligned} R(x) &= \frac{-Q_1 \sin P(L-x)}{iP \operatorname{sgn}\left(P^2\right) \cos PL + Q_2 \sin PL}, \\ T(x) &= \frac{iP \operatorname{sgn}\left(P^2\right) \cos P(L-x) + Q_2 \sin P(L-x)}{iP \operatorname{sgn}\left(P^2\right) \cos PL + Q_2 \sin PL}. \end{aligned}\right\} \tag{B19}$$

For $P^2 > 0$:

$$\left.\begin{aligned} R(x) &= \frac{-Q_1 \sin P(L-x)}{iP \cos PL + Q_2 \sin PL}, \\ T(x) &= \frac{iP \cos P(L-x) + Q_2 \sin P(L-x)}{iP \cos PL + Q_2 \sin PL}. \end{aligned}\right\} \tag{B20}$$

For $P^2 < 0$: P is a pure imaginary number. By introducing a real parameter, $P_b = iP$, the solutions are

$$\left.\begin{aligned} R(x) &= \frac{-iQ_1 \sinh P_b(L-x)}{iP_b \cosh P_b L - Q_2 \sinh P_b L}, \\ T(x) &= \frac{iP_b \cosh P_b(L-x) - Q_2 \sinh P_b(L-x)}{iP_b \cosh P_b L - Q_2 \sinh P_b L}. \end{aligned}\right\} \tag{B21}$$

For $P^2 = 0$: We take $P \to 0$ in (B20) to obtain

$$\left.\begin{aligned} R(x) &= \frac{-Q_1(L-x)}{i + Q_2 L}, \\ T(x) &= \frac{i + Q_2(L-x)}{i + Q_2 L}. \end{aligned}\right\} \tag{B22}$$

In summary, reflectance $\tilde{R}$ and transmittance $\tilde{T}$ can be expressed as follows:

$$\left.\begin{aligned} \tilde{R} &= |R(0)| = \sqrt{\frac{Q_1^2}{|P \cot PL|^2 + Q_2^2}}, \\ \tilde{T} &= |T(L)| = \sqrt{\frac{|P|^2}{|P \cot PL|^2 + Q_2^2 |\sin PL|^2}}. \end{aligned}\right\} \tag{B23}$$

Appendix C. Magnitude of the downshift of the wave frequency

Assuming that the magnitude of the frequency shift δ is small, i.e. $\delta \ll O(1)$, we can demonstrate that $P^2 < 0$, resulting in the substitution of $|P \cot PL|$ with $iP_b \cosh P_b L$, with $P_b = iP$, as detailed in Appendix B. Combining (3.10) with (3.5) then provides an implicit

relation for δ as follows:

$$\Gamma\left(\omega', D\right)\big|_{\omega'=\delta} = 0, \tag{C1}$$

in which $\Gamma(\omega', D)$ is a binary function on ω' and D, defined as

$$\Gamma\left(\omega', D\right) = 2\left\{Q_2^2 + (iP_b \cosh P_b L)^2\right\}\frac{\partial Q_1}{\partial \omega'} - Q_1\left\{\frac{\partial Q_2^2}{\partial \omega'} + \frac{\partial (iP_b \cosh P_b L)^2}{\partial \omega'}\right\}. \tag{C2}$$

Applying the first-order Taylor expansion to Γ in terms of ω' results in

$$\Gamma(\delta, D) = \Gamma(0, D) + \frac{\partial \Gamma(0, D)}{\partial \omega'}\delta + O\left(\delta^2\right) = 0, \tag{C3}$$

which leads to an approximate explicit solution for δ by eliminating the high-order error,

$$\delta = \Lambda(D) + O(\delta) \approx \Lambda(D), \tag{C4}$$

in which $\Lambda(D)$ is a function relying on D

$$\Lambda(D) = -\left(\frac{\partial \log |\Gamma(0, D)|}{\partial \omega'}\right)^{-1}. \tag{C5}$$

It is necessary to further simplify the highly intricate expression of $\Lambda(D)$. This can be done through the application of a second-order Taylor expansion, expressed as follows:

$$\Lambda(D) \approx \delta_0 + \delta_1 D + \delta_2 D^2 + O\left(D^3\right), \tag{C6}$$

where $\delta_1 = \mathrm{d}\Lambda(0)/\mathrm{d}D = 0$. Let δ_0 and $2\delta_2$ represent $\Lambda(0)$ and $\mathrm{d}^2\Lambda(0)/\mathrm{d}D^2$, respectively. We have

$$\delta_0 = \frac{3iC_g^+\left(E_3 + iE_1 C_g^+\right)}{6E_2 E_3 C_g^+ - iL^2 D_0^+}, \tag{C7}$$

and

$$\delta_2 = \frac{\eth_4 L^4 + \eth_2 L^2}{5C_g^+\left(6E_2 E_3 C_g^+ - iL^2 D_0^+\right)^2}, \tag{C8}$$

in which $\eth_4$ and $\eth_2$ are defined in (3.12) and (3.13). Thus, an approximate solution for the frequency downshift of the Bragg resonance is expressed as

$$\delta = \frac{3iC_g^+\left(E_3 + iE_1 C_g^+\right)}{6E_2 E_3 C_g^+ - iL^2 D_0^+} + \frac{\eth_4 L^4 + \eth_2 L^2}{5C_g^+\left(6E_2 E_3 C_g^+ - iL^2 D_0^+\right)^2}. \tag{C9}$$

Appendix D. Expressions for the operators

The first-order operators are defined as

$$\bar{\mathcal{L}}_{flu}\left[\gamma_{1,1}^{1,\pm}S_{1,1}^{\pm}\right] = \frac{T_{1,1}^{1,\pm}(z+h)\sinh k(z+h)}{2k\cosh k(z+h)}, \tag{D1}$$

and we have

$$\left.\begin{aligned}
\bar{\mathcal{L}}_{bot}\left[\gamma_{1,1}^{1,-}S_{1,1}^{-}\right] &= \left[De^{2ikx}\left(-\frac{1}{2}\frac{\partial^2}{\partial z^2}+ik\frac{\partial}{\partial x}\right)\gamma_{1,1}^{1,-}S_{1,1}^{-}\bigg|_{z=-h}\right]\frac{\sinh k(z+h)}{k}, \\
\bar{\mathcal{L}}_{bot}\left[\gamma_{1,1}^{1,+}S_{1,1}^{+}\right] &= \bar{\mathcal{L}}_{bot}^{(1)}\left[\gamma_{1,1}^{1,+}S_{1,1}^{+}\right]+\bar{\mathcal{L}}_{bot}^{(2)}\left[\gamma_{1,1}^{1,+}S_{1,1}^{+}\right],
\end{aligned}\right\} \tag{D2}$$

and

$$\left.\begin{aligned}
\bar{\mathcal{L}}_{bot}^{(1)}\left[\gamma_{1,1}^{1,+}S_{1,1}^{+}\right] &= \left[De^{-2ikx}\left(-\frac{1}{2}\frac{\partial^2}{\partial z^2}+ik\frac{\partial}{\partial x}\right)\gamma_{1,1}^{1,+}S_{1,1}^{+}\bigg|_{z=-h}\right]\frac{\sinh k(z+h)}{k}, \\
\bar{\mathcal{L}}_{bot}^{(2)}\left[\gamma_{1,1}^{1,+}S_{1,1}^{+}\right] &= \left[De^{2ikx}\left(-\frac{1}{2}\frac{\partial^2}{\partial z^2}-ik\frac{\partial}{\partial x}\right)\gamma_{1,1}^{1,+}S_{1,1}^{+}\bigg|_{z=-h}\right]\left\{\frac{\sinh 3k(z+h)}{3k}\right. \\
&\quad\left.+\frac{\omega^2\tanh 3kh-3gk}{9gk^2\tanh 3kh-3k\omega^2}\cosh 3k(z+h)\right\},
\end{aligned}\right\} \tag{D3}$$

in which the superscripts (1) and (2) are the operator generating modes $S_{1,1}^{-}$ and $S_{3,1}^{+}$, respectively.

For the second-order operators, we have

$$\left.\begin{aligned}
\mathcal{L}_{flu}\left[\phi_1,\phi_2\right] &= -\int_{-h}^{0}\left(-\frac{\partial^2\phi_1}{\partial\xi_1^2}-2\frac{\partial^2\phi_2}{\partial x\partial\xi_1}\right)\psi^+\,dz, \\
\mathcal{L}_{sur}\left[\phi_1,\phi_2\right] &= \left(-\frac{\partial^2\phi_1}{\partial\tau_1^2}-2\frac{\partial^2\phi_2}{\partial t\partial\tau_1}\right)\frac{\psi^+}{g}\bigg|_{z=0},
\end{aligned}\right\} \tag{D4}$$

and

$$\mathcal{L}_{bot}\left[\phi_1,\phi_2\right] = \zeta\left\{-\left[\frac{\partial\sigma}{\partial x}\frac{\partial\phi_1}{\partial\xi_1}+\left(\frac{\partial\sigma}{\partial x}\frac{\partial}{\partial x}-\sigma\frac{\partial^2}{\partial z^2}\right)\phi_2\right]\psi^+\bigg|_{z=-h}\right\}, \tag{D5}$$

which are bilinear operators on ϕ_1, the component at $O(\varepsilon)$, and ϕ_2, at $O(\varepsilon^2)$. In addition, ζ is the operator to take out the terms related to the mode $S_{1,1}^{+}$.

Appendix E. Numerical solution procedure for the ENLS

Substituting (4.1) and (4.2) into (2.42) and (2.43), and separating real and imaginary items, we have

$$\frac{dY(x)}{dx} = \wp(x), \tag{E1}$$

in which

$$Y(x) = (R_{re}, R_{im}, T_{re}, T_{im})^T, \tag{E2}$$

$$\wp(x) = \begin{pmatrix} S_3^+ & 0 & S_4^+ & 0 \\ 0 & -S_3^+ & 0 & -S_4^+ \\ S_4^+ & 0 & S_3^+ & 0 \\ 0 & S_4^+ & 0 & S_3^+ \end{pmatrix}^{-1} \left\{ -\begin{pmatrix} iS_1^+ R_{im} + iS_2^+ T_{im} \\ iS_1^+ R_{re} + iS_2^+ T_{re} \\ -iS_2^+ R_{im} - iS_1^+ T_{im} \\ iS_2^+ R_{re} + iS_1^+ T_{re} \end{pmatrix} + \wp_n(x) \right\}, \tag{E3}$$

and $\wp_n(x)$ is the nonlinear contribution,

$$\wp_n(x) = -iA_0^2 \begin{pmatrix} T_{im} \left\{ F_2^+ \left(R_{im}^2 + R_{re}^2 \right) + F_1^+ \left(T_{im}^2 + T_{re}^2 \right) \right\} \\ T_{re} \left\{ F_2^+ \left(R_{im}^2 + R_{re}^2 \right) + F_1^+ \left(T_{im}^2 + T_{re}^2 \right) \right\} \\ -R_{im} \left\{ F_1^+ \left(R_{im}^2 + R_{re}^2 \right) + F_2^+ \left(T_{im}^2 + T_{re}^2 \right) \right\} \\ R_{re} \left\{ F_1^+ \left(R_{im}^2 + R_{re}^2 \right) + F_2^+ \left(T_{im}^2 + T_{re}^2 \right) \right\} \end{pmatrix}. \tag{E4}$$

According to (B8), the boundary conditions give

$$T_{re}(0) = 1, \quad T_{im}(0) = 0, \quad R_{re}(L) = 0, \quad R_{im}(L) = 0. \tag{E5}$$

For a specific frequency ω' and wave amplitude of incident wave A_0, the nonlinear system of ordinary differential equations (E1) with boundaries (E5) forms a well-defined BVP. We adopt a fourth-order Runge–Kutta method with a step size of $\Delta x = L/N_t$, with N_t fixed to 10^4, to discretise the governing equation. We denote by x^n the discrete points on $[0, L]$, where $x^n = (n-1)\Delta x$, $(1 \le n \le N_t + 1)$, and $Y(x_n)$ and $\wp(x_n)$ are defined as Y^n and $\wp^n$, respectively. To evaluate the error of the numerical solutions, we introduce an indicator:

$$\text{err} = \sum_{n=1}^{N_t} \left| \frac{Y^{n+1} - Y^n}{\Delta x} - \wp^n \right|^2 \frac{\Delta x}{L}, \tag{E6}$$

which represents the global squared error of the numerical solution on $[0, L]$. Each incident wave frequency and wave amplitude correspond to an error. Thus, err_{max} can be used to characterise the maximum error

$$\text{err}_{max} = \max_{A_0, \omega'} \{\text{err}\}. \tag{E7}$$

By choosing this discrete format, the accuracy of the numerical solutions can be guaranteed, with $\text{err}_{max} < 10^{-6}$.

REFERENCES

AKHMEDIEV, N., ANKIEWICZ, A. & TAKI, M. 2009 Waves that appear from nowhere and disappear without a trace. *Phys. Lett.* A **373** (6), 675–678.

ARDHUIN, F. & HERBERS, T.H.C. 2002 Bragg scattering of random surface gravity waves by irregular seabed topography. *J. Fluid Mech.* **451**, 1–33.

ARDHUIN, F. & MAGNE, R. 2007 Scattering of surface gravity waves by bottom topography with a current. *J. Fluid Mech.* **576**, 235–264.

BENJAMIN, T.B. & FEIR, J.E. 1967 The disintegration of wave trains on deep water. Part 1. Theory. *J. Fluid Mech.* **27** (3), 417–430.

BERKHOFF, J.C.W. 1973 Computation of combined refraction–diffraction. *Coast. Engng* **1972**, 471–490.

CHAMBERLAIN, P.G. & PORTER, D. 1995 The modified mild-slope equation. *J. Fluid Mech.* **291**, 393–407.

DAVIES, A.G. & HEATHERSHAW, A.D. 1984 Surface-wave propagation over sinusoidally varying topography. *J. Fluid Mech.* **144**, 419–443.

DHAR, A.K. & KIRBY, J.T. 2023 Fourth-order stability analysis for capillary-gravity waves on finite-depth currents with constant vorticity. *Phys. Fluids* **35** (2), 026601.

FANG, H., TANG, L. & LIN, P. 2023 Homotopy analysis of wave transformation over permeable seabeds and porous structures. *Ocean Engng* **274**, 114087.

FRANCIUS, M. & KHARIF, C. 2017 Two-dimensional stability of finite-amplitude gravity waves on water of finite depth with constant vorticity. *J. Fluid Mech.* **830**, 631–659.

GAO, J., MA, X., DONG, G., CHEN, H., LIU, Q. & ZANG, J. 2021 Investigation on the effects of Bragg reflection on harbor oscillations. *Coast. Engng* **170**, 103977.

GUAZZELLI, E., REY, V. & BELZONS, M. 1992 Higher-order Bragg reflection of gravity surface waves by periodic beds. *J. Fluid Mech.* **245**, 301–317.

HAMMACK, J.L., HENDERSON, D.M. & SEGUR, H. 2005 Progressive waves with persistent two-dimensional surface patterns in deep water. *J. Fluid Mech.* **532**, 1–52.

HARA, T. & MEI, C.C. 1988 Bragg scattering of surface waves by periodic bars: theory and experiment. *J. Fluid Mech.* **178**, 221–241.

HOWARD, L.N. & YU, J. 2007 Normal modes of a rectangular tank with corrugated bottom. *J. Fluid Mech.* **593**, 209–234.

KIRBY, J.T. 1986*a* A general wave equation for waves over rippled beds. *J. Fluid Mech.* **162**, 171–186.

KIRBY, J.T. 1986*b* On the gradual reflection of weakly nonlinear Stokes waves in regions with varying topography. *J. Fluid Mech.* **162**, 187–209.

KIRBY, J.T. 1988 Current effects on resonant reflection of surface water waves by sand bars. *J. Fluid Mech.* **186**, 501–520.

KIRBY, J.T. 1993 A note on Bragg scattering of surface waves by sinusoidal bars. *Phys. Fluids* A **5** (2), 380–386.

KIRBY, J.T. & ANTON, J.P. 1990 Bragg reflection of waves by artificial bars. *Coast. Engng* **1990**, 757–768.

KIRBY, J.T. & DALRYMPLE, R.A. 1983 A parabolic equation for the combined refraction–diffraction of Stokes waves by mildly varying topography. *J. Fluid Mech.* **136**, 453–466.

KIRBY, J.T. & DALRYMPLE, R.A. 1984 Verification of a parabolic equation for propagation of weakly-nonlinear waves. *Coast. Engng* **8** (3), 219–232.

LAFFITTE, E., REY, V., TOUBOUL, J. & BELIBASSAKIS, K. 2021 Water wave scattering by a sinusoidal bed in the presence of vertically sheared current. *Appl. Ocean Res.* **108**, 102549.

LAKE, B.M., YUEN, H.C., RUNGALDIER, H. & FERGUSON, W.E. 1977 Nonlinear deep-water waves: theory and experiment. Part 2. Evolution of a continuous wave train. *J. Fluid Mech.* **83** (1), 49–74.

LIANG, B., GE, H., ZHANG, L. & LIU, Y. 2020 Wave resonant scattering mechanism of sinusoidal seabed elucidated by Mathieu instability theorem. *Ocean Engng* **218**, 108238.

LIAO, B., DONG, G., MA, Y. & GAO, J.L. 2017 Linear-shear-current modified Schrdinger equation for gravity waves in finite water depth. *Phys. Rev.* E **96** (4), 043111.

LIU, H.W., LI, X.F. & LIN, P.Z. 2019 Analytical study of Bragg resonance by singly periodic sinusoidal ripples based on the modified mild-slope equation. *Coast. Engng* **150**, 121–134.

LIU, H.-W., LUO, H. & ZENG, H.-D. 2015 Optimal collocation of three kinds of Bragg breakwaters for Bragg resonant reflection by long waves. *ASCE J. Waterway Port Coastal Ocean Engng* **14** (3), 04014039.

LIU, H.W. & ZHOU, X.M. 2014 Explicit modified mild-slope equation for wave scattering by piecewise monotonic and piecewise smooth bathymetries. *J. Engng Mech.* **87** (1), 29–45.

LIU, P.L.F. & TSAY, T.K. 1984 Refraction-diffraction model for weakly nonlinear water waves. *J. Fluid Mech.* **141**, 265–274.

LIU, Y. & YUE, D.K.P. 1998 On generalized Bragg scattering of surface waves by bottom ripples. *J. Fluid Mech.* **356**, 297–326.

MADSEN, P.A., FUHRMAN, D.R. & WANG, B. 2005 A Boussinesq-type method for fully nonlinear waves interacting with a rapidly varying bathymetry. *Coast. Engng* **53** (5–6), 487–504.

MAGNE, R., REY, V. & ARDHUIN, F. 2005 Measurement of wave scattering by topography in the presence of currents. *Phys. Fluids* **17** (12), 126601.

MEI, C.C. 1985 Resonant reflection of surface water waves by periodic sandbars. *J. Fluid Mech.* **152**, 315–335.

MEI, C.C., HARA, T. & NACIRI, M. 1988 Note on Bragg scattering of water waves by parallel bars on the seabed. *J. Fluid Mech.* **186**, 147–162.

ONORATO, M., OSBORNE, A.R. & SERIO, M. 2006 Modulational instability in crossing sea states: a possible mechanism for the formation of freak waves. *Phys. Rev. Lett.* **96** (1), 014503.

PENG, J., TAO, A, LIU, Y., ZHENG, J., ZHANG, J. & WANG, R. 2019 A laboratory study of class III Bragg resonance of gravity surface waves by periodic beds. *Phys. Fluids* **31**, 067110.

PIZZO, N., LENAIN, L., RØMCKE, O., ELLINGSEN, S.Å. & SMELTZER, B.K. 2023 The role of Lagrangian drift in the geometry, kinematics and dynamics of surface waves. *J. Fluid Mech.* **954**, R4.

REY, V., GUAZZELLI, É. & MEI, C.C. 1996 Resonant reflection of surface gravity waves by one-dimensional doubly sinusoidal beds. *Phys. Fluids* **8** (6), 1525–1530.

THOMAS, R., KHARIF, C. & MANNA, M. 2012 A nonlinear Schrödinger equation for water waves on finite depth with constant vorticity. *Phys. Fluids* **24** (12), 127102.

WANG, Z., GUAN, X. & VANDEN-BROECK, J.M. 2020 Progressive flexural–gravity waves with constant vorticity. *J. Fluid Mech.* **905**, A12.

YU, J. & HOWARD, L.N. 2012 Exact Floquet theory for waves over arbitrary periodic topographies. *J. Fluid Mech.* **712**, 451–470.